# Analysis of X-ray Absorption Spectra of Some Nickel Oxycompounds Using Theoretical Standards

**A. N. Mansour***

*Naval Surface Warfare Center, Carderock Division, Code 684, 9500 MacArthur Boulevard, West Bethesda, Maryland 20817-5700*

**C. A. Melendres**

*Argonne National Laboratory, Materials Science and Chemical Technology Divisions, 9700 South Cass Avenue, Argonne, Illinois 60439-8111*

*Received: July 3, 1996; In Final Form: October 31, 1997*[⊗]

X-ray absorption spectra have been measured for NiO, $\beta$-$Ni(OH)_2$, $\alpha$-$Ni(OH)_2$, $LiNiO_2$, and $KNiIO_6$ samples, which contain nickel with valency in the range 2−4. Information on the local structure and nature of bonding of nickel compounds has been derived using theoretical standards generated with the FEFF code. The Ni K-edge energy was found to shift to higher values by about 1.5 eV per unit change in valency of nickel. The energy of the preedge peak (generally attributed to the transition from the 1s core states to the 3d unoccupied states) shifts to higher values by about 0.6 eV per unit change in valency of nickel. A many body amplitude reduction factor ($S_0^2$) of 0.77 ± 0.03 for Ni K-edge absorption can be used to scale theoretical spectra to fit the experimental ones in order to accurately determine the coordination numbers for compounds with complex structures. Our results show that chemical effects are very small and can be ignored for reliable structural analysis. Results of local structure for the first, second, and third coordination spheres for NiO are consistent with those derived from X-ray diffraction data. The results for $\beta$-$Ni(OH)_2$ are much closer in agreement with those derived from the neutron diffraction data rather than the X-ray diffraction data. The results for $\alpha$-$Ni(OH)_2$ differ significantly from those based on the idealized structure model proposed by Bode et al. In fact, the structure within the hexagonal planes for $\alpha$-$Ni(OH)_2$ is similar to that for $\beta$-$Ni(OH)_2$. The apparent contraction in the Ni−Ni distance of the third coordination sphere for $\alpha$-$Ni(OH)_2$ relative to that for $\beta$-$Ni(OH)_2$, which was previously reported by others, is not real and can be attributed to structural disorder. The Ni−O bond length for divalent nickel with an octahedral coordination is in the range 2.06−2.08 Å. The first coordination sphere for $LiNiO_2$ consists of four and two oxygens at 1.91 and 2.06 Å, respectively, rather than six oxygens at 2.04 Å, as predicted by the X-ray diffraction data. The short distance is characteristic of $Ni^{3+}-O^{2-}$ bonds and $Ni^{2+}-O^{-}$ bonds, while the long distance is characteristic of $Ni^{2+}-O^{2-}$ bonds. The local structure for $LiNiO_2$ is consistent with the fact that the charge-compensating mechanism is largely due to oxygen 2p holes. The Ni−Ni second-shell distance for $LiNiO_2$ is consistent with that based on the X-ray and neutron diffraction data. The Ni−O bond length for quadrivalent Ni in $KNiIO_6$ is 1.88 Å. The Ni−O bond length varies with nickel valency in a nonlinear manner.

## Introduction

The structure and composition of the higher oxides and hydroxides of nickel are of great interest from the standpoint of a number of technological applications, e.g., advanced nickel batteries, electrochromic devices, and corrosion protection. Despite the considerable research work that has been carried out, there is still much uncertainty and confusion as to the stoichiometry and structure of the various oxides (hydroxides) that are formed, for example, during the charging (and discharging) of the nickel oxide electrode in nickel batteries.[1] The difficulty in probing their structure stems, in part, from the highly disordered or amorphous nature of the phases formed, which makes structural determination by X-ray diffraction difficult. Furthermore, the oxidation states of Ni in these compounds are still the subject of much controversy and need clarification. X-ray absorption spectroscopy (XAS) is an excellent technique for characterizing the valency and local structure of Ni in such materials with no long-range order.[2] There have been a number of studies that used XAS to characterize the local structure and valency of nickel in oxycompounds as well as the nickel oxide electrode. Crespin, Levitz, and Gatineau[3] used XAS to examine the chemistry and structure of intermediate phases formed during the low-temperature reduction of $LaNiO_3$; they observed that the X-ray absorption edge energy correlates very well with changes in nickel valency from 1 to 3. Levitz, Crespin, and Gatineau[4] also examined the structure of monovalent Ni in $LaNiO_2$. McBreen et al.[5] carried out an "in situ" XAS study to monitor changes in the local structure of Ni upon charging and discharging $Ni(OH)_2$ containing 5 wt % $Co(OH)_2$ in 8.4 M KOH + 0.5 M LiOH electrolyte. They observed an octahedral coordination

* To whom all correspondence should be sent at the following address: Carderock Division, Naval Surface Warfare Center, Code 684, Bldg. 19-A250, 9500 MacArthur Blvd., West Bethesda, MD 20817-5700.

⊗ Abstract published in *Advance ACS Abstracts,* December 15, 1997.

S1089-5639(96)01985-8 CCC: $15.00 
Published on Web 01/01/1998

as well as a contraction in the Ni−O distance from 2.04 to 1.88 Å upon charging $Ni(OH)_2$ to the trivalent state. In a similar experiment, Pandya et al.[6] carried out an "in situ" investigation to examine the structural changes during the charge and discharge cycles of $\beta$-$Ni(OH)_2$ containing 5 wt % $Co(OH)_2$. In this experiment, they observed that the first coordination sphere of Ni in the charged state consists of four oxygen atoms at 1.88 Å and two oxygen atoms at 2.07 Å. They speculated that the long Ni−O distance may indicate incomplete oxidation of $\beta$-$Ni(OH)_2$ or that some self-discharge occurred. However, the authors stated that due to the reproducibility of this effect in various cells and after repeated discharge−charge cycles, the two different Ni−O distances indicate a distorted octahedral coordination for single-phase Ni in the charged state; this distortion was assumed to be characteristic of trivalent Ni. McBreen et al.[7] conducted an "in situ" time-resolved XAS study coupled with cyclic voltammetry to investigate the XANES of Ni during the charge and discharge of $\alpha$-$Ni(OH)_2$ and $\beta$-$Ni(OH)_2$ in KOH electrolyte. They observed a continuous shift in the Ni K-edge energy, which they asserted was consistent with the electrochemical oxidation of $Ni^{2+}$ to $Ni^{3+}$. Pandya et al.[8] examined the local structure of both $\alpha$-$Ni(OH)_2$ and $\beta$-$Ni(OH)_2$. They claimed that the Ni−Ni distance of the second coordination sphere for $\alpha$-$Ni(OH)_2$ is shorter than that for $\beta$-$Ni(OH)_2$ by 0.05 Å. In addition, they asserted an increase in the number of Ni−O bonds in $\alpha$-$Ni(OH)_2$ upon hydration. Capehart et al.,[9] using thin films of $Ni(OH)_2$ deposited on a gold-coated plastic substrate by cathodic precipitation, claimed to have charged the nickel oxide electrode to a state where the average nickel valency was 3.67 and thus postulated the formation of a $K(NiO_2)_3$ phase. In this phase, the Ni−O bond length was determined to be 1.86 Å, and the average valency of Ni was estimated from the dependence of the Ni−O bond length on Ni valency which was deduced from structure data for NiO, $\beta$-$Ni(OH)_2$, and $\beta$-NiOOH. Recently, Mansour et al.[10] examined the XANES spectra of NiO, $Ni_3O_2(OH)_4$, $\beta$-NiOOH, commercially obtained "$NiO_2$", and $KNiIO_6$. In this study, the XANES of quadrivalent Ni was reported for the first time, and the authors observed that the X-ray edge energy linearly increased with increase in valency of nickel from 0 to 4. Based on the X-ray edge energies, it was concluded that $Ni_3O_2(OH)_4$, $\beta$-NiOOH, and "$NiO_2$" contain nickel in the trivalent state. More recently, in preliminary reports, Mansour et al.[11] and Mansour and Melendres[12,13] reported on the local structure of Ni in NiO, $\beta$-$Ni(OH)_2$, $Ni_3O_2(OH)_4$, $\beta$-NiOOH, $\gamma$-NiOOH, $NiO_2$, and $KNiIO_6$. The Ni−O bond length of $Ni^{4+}$ in $KNiIO_6$ as determined from X-ray absorption spectra was also reported by Curie et al.[14] Later on, O'Grady et al.[15] reported the XANES and local structure of quadrivalent Ni in $BaNiO_3$ and claimed the presence of $Ni^{4+}$ in a charged nickel oxide electrode.

In many of the nickel oxyhydroxides such as $\beta$- and $\gamma$-NiOOH, the structure of the first coordination sphere of Ni−O could only be analyzed in terms of two Ni−O bond lengths; a short one, near 1.88 Å, is close to that for $Ni^{4+}$, and a long one, near 2.06 Å, is close to that for $Ni^{2+}$. Thus, to account for both the short and long Ni−O bond lengths, the structure of the higher valency oxyhydroxides can be interpreted in terms of two different models. One model, which was adapted in earlier work,[6] assumes that the material consists of trivalent Ni with a distorted octahedral coordination. The other model that we proposed,[11−13] is that the material consists of two phases. One phase contains $Ni^{4+}$ with a short Ni−O bond length of ≈1.88 Å, similar to that in $KNiIO_6$. The other phase contains $Ni^{2+}$ with a Ni−O bond length of ≈2.06 Å, similar to that in $\beta$-$Ni(OH)_2$. To differentiate between these two models, the local structure of nickel in reference compounds with known valency must be established. In this investigation, we used XAS to study a number of nickel oxycompounds with well-defined XRD and/or neutron diffraction patterns. We measured the room-temperature X-ray absorption spectra of Ni, NiO, $\beta$-$Ni(OH)_2$, $\alpha$-$Ni(OH)_2$, $LiNiO_2$, and $KNiIO_6$. The investigated compounds shall serve as references for further room-temperature "ex situ" and "in situ" XAS studies of the higher oxide forms of nickel such as the $\beta$- and $\gamma$-NiOOH, nickel oxide thin films, and $LiNiO_2$ electrodes. Detailed analysis of the local structure up to the third coordination sphere was made using theoretical standards generated with the FEFF code rather than empirical standards, as had been done in most of the earlier work. We show that the EXAFS results are in excellent agreement with those of XRD for Ni and NiO and neutron diffraction for $\beta$-$Ni(OH)_2$. For $\alpha$-$Ni(OH)_2$, we will show that the local structure for nickel within the hexagonal planes is similar to that of Ni in $\beta$-$Ni(OH)_2$ except for an increase in disorder in $\alpha$-$Ni(OH)_2$ relative to that in $\beta$-$Ni(OH)_2$. For $LiNiO_2$ and $KNiIO_6$, the results for the Ni−Ni or Ni−I atom pair are consistent with results based on XRD, while those for the first shell of the Ni−O atom pair differed significantly from those based on XRD. Finally, we establish calibration curves based on the Ni K-edge energies, the Ni−O first-shell distance, and nickel valency, which can be used to infer the nickel valency in other nickel oxycompounds with complex structures.

## Experimental Section

**Sample Preparation.** Most of the compounds studied were prepared by chemical synthesis following procedures established in the literature; others were purchased from commercial suppliers. Research grade high purity NiO and $\beta$-$Ni(OH)_2$ materials were obtained commercially from Aldrich Chemical Co. (Milwaukee, WI) and McGean Chemical Co. (Cleveland, OH), respectively. The $\alpha$-$Ni(OH)_2$ sample was made by reacting $Ni(NO_3)_2$ with NaOH following the procedure described by Glemser.[16] Thermogravimetric analysis of this $\alpha$-$Ni(OH)_2$ sample showed the composition to be $3Ni(OH)_2 \cdot 2H_2O$, which is consistent with its X-ray diffraction pattern, which will be discussed later in the text. The $LiNiO_2$ material was obtained from Rayovac Co. (Madison, WI). This material was synthesized using LiOH and $Ni(OH)_2$ as precursors.[17] The $KNiIO_6$ sample was synthesized following the procedure of Murthy[18] for the peroxydisulfate oxidation of a solution of $NiSO_4 + KIO_4$. A high-purity (99.95%) 4 $\mu$m thick Ni foil was purchased from Goodfellow (Cambridge Science Park, U.K.).

**X-ray Diffraction Measurements.** The X-ray diffraction measurements were collected using monochromatized Cu K$\alpha$ X-rays from a Siemens Model Diffrac 500 unit. Powder X-ray diffraction (XRD) patterns were obtained in order to confirm the purity of the materials. The XRD pattern for NiO showed single-phase material and was consistent with published data (ICDD powder diffraction file 4-835). The XRD pattern for the $\beta$-$Ni(OH)_2$ sample was similar to the well-established pattern for $\beta$-$Ni(OH)_2$ (ICDD powder diffraction file 14-177). The XRD pattern for $\alpha$-$Ni(OH)_2$ differed from that for $\beta$-$Ni(OH)_2$. It showed broad peaks with weak intensities, and the $2\theta$-coordinate of the (003) reflection indicates a significant degree of disorder due to hydration. Specifically, this XRD pattern is similar to that of a hydrated nickel hydroxide sample with a composition of $Ni(OH)_2 \cdot 0.75H_2O$ (ICDD powder diffraction file 38−715) in agreement with thermogravimetric analysis which yielded a composition of $Ni(OH)_2 \cdot 0.67H_2O$ for our sample. The

**TABLE 1: Summary of Structural Parameters from X-ray Diffraction and Neutron Diffraction Data.**

| compound | lattice & space group | unit cell dimensions (Å) | local structure X-Y pair | *N* | *R* (Å) | ref |
|---|---|---|---|---|---|---|
| Ni | cubic ($Fm$-3$m$) | $a = 3.5239$ | Ni−Ni | 12 | 2.492 | 20 |
| NiO | cubic ($Fm$-3$m$) | $a = 4.1770$ | Ni−O | 6 | 2.089 | 21 |
| | | | Ni−Ni | 12 | 2.954 | |
| | | | Ni−O | 8 | 3.617 | |
| $\beta$-Ni(OD)$_2$ (neutron diffraction) | hexagonal ($P$-3$m$1) | $a = 3.126$ $c = 4.593$ | Ni−O | 6 | 2.073 | 22 |
| | | | Ni−D | 6 | 2.667 | |
| | | | Ni−Ni | 6 | 3.126 | |
| | | | Ni−O | 6 | 3.751 | |
| $\beta$-Ni(OH)$_2$ (neutron diffraction) | hexagonal ($P$-3$m$1) | $a = 3.119$ $c = 4.686$ | Ni−O | 6 | 2.080 | 22 |
| | | | Ni−H | 6 | 2.784 | |
| | | | Ni−Ni | 6 | 3.119 | |
| | | | Ni−O | 6 | 3.749 | |
| $\beta$-Ni(OH)$_2$ | hexagonal ($P$-3$m$1) | $a = 3.1260$ $c = 4.6050$ | Ni−O | 6 | 2.141 | 23 |
| | | | Ni−H | 6 | 2.587 | |
| | | | Ni−Ni | 6 | 3.126 | |
| | | | Ni−O | 6 | 3.789 | |
| $\alpha$-Ni(OH)$_2$·0.67H$_2$O | hexagonal ($P$-31$m$) | $a = 5.340$ $c = 8.090$ | Ni−O | 6 | 2.233 | 24 |
| | | | Ni−H | 6 | | |
| | | | Ni−Ni | 6 | 3.083 | |
| | | | Ni−O | 6 | 3.807 | |
| LiNiO$_2$ | hexagonal ($R$-3$m$) | $a = 2.8823$ $c = 14.2085$ | Ni−O | 6 | 2.042 | 25, 26 |
| | | | Ni−Ni | 6 | 2.882 | |
| | | | Ni−Li | 6 | 2.894 | |
| Li$_{0.4}$Ni$_{0.6}$O (neutron diffraction) | hexagonal ($R$-3$m$) | $a = 2.8861$ $c = 14.1924$ | Ni−O | 6 | 1.985 | 30 |
| | | | Ni−Ni | 6 | 2.890 | |
| | | | Ni−Li | 6 | 2.898 | |
| KNiIO$_6$ | hexagonal ($P$312) | $a = 4.9690$ $c = 6.0220$ | Ni−O | 6 | 1.796 | 27, 28 |
| | | | Ni−I | 3 | 2.869 | |
| | | | Ni−O | 6 | 3.470 | |
| KNiIO$_6$ | hexagonal ($P$312) | $a = 4.969$ $c = 6.00$ | Ni−O | 6 | 2.176 | 29 |
| | | | Ni−I | 3 | 2.869 | |
| | | | Ni−O | 6 | 3.449 | |

XRD pattern for LiNiO$_2$ displayed sharp peaks and is consistent with published data (ICDD powder diffraction file 9-63). Our LiNiO$_2$ XRD pattern is similar to that of an LiNiO$_2$ sample prepared using preparation method "D" described by Ohzuku et al.[19] The LiNiO$_2$ material prepared by this method had the highest electrochemical reactivity compared to material prepared by other methods. The XRD pattern for KNiIO$_6$ indicated also a well-crystallized single-phase material with sharp diffraction peaks.[10]

To aid in the analysis of XAS data, nickel local structure parameters as well as lattice type, space group, and unit cell dimensions are listed in Table 1 for Ni,[20] NiO,[21] $\beta$-Ni(OD)$_2$ and $\beta$-Ni(OH)$_2$ based on neutron diffraction data[22] and XRD data,[23] $\alpha$-Ni(OH)$_2$,[24] LiNiO$_2$,[25,26] and KNiIO$_6$.[27,28] Structural parameters for KNiIO$_6$ based on more recent XRD data were also included.[29] The XRD data for LiNiO$_2$ are consistent with neutron diffraction data for an Li$_{0.4}$Ni$_{0.6}$O sample which is closely related in composition with our sample except for a difference in the position of the oxygen atoms.[30] The Ni−O bond length based on neutron diffraction data for Li$_{0.4}$Ni$_{0.6}$O is 1.99 Å in contrast to 2.04 Å for LiNiO$_2$ based on XRD data (see Table 1). Structural data for $\alpha$-Ni(OH)$_2$ were based on an idealized structure model for a sample with composition 3Ni(OH)$_2$·2H$_2$O, which contains two nonequivalent Ni sites; the data in Table 1 represent the weighted average from structure data for both sites.

**XAS Measurements.** The X-ray absorption experiments were performed on beamline X-11A of the National Synchrotron Light Source (NSLS) at Brookhaven National Laboratory (BNL) with the electron storage ring operating at an electron energy of 2.584 GeV and a stored current in the range 110−300 mA.[31] Data were collected with a variable exit double-crystal monochromator using two flat Si(111) crystals. The estimated energy resolution for this monochromator taking into account the incident beam slit width of 0.5 mm at a distance of 10 m from the source is in the range 1.9−2.7 eV throughout the Ni K-edge spectrum. Harmonics were rejected by detuning the parallelism of the monochromator crystals. The X-ray intensities were monitored using ionization chambers filled with nitrogen gas for the incident beam and a mixture of argon (15%) and nitrogen (85%) gases for the transmitted beam. Spectra of the Ni K-edge (8333 eV) were obtained at room temperature (300 K) in transmission using the step-by-step scanning mode. Data were collected with an energy per step interval of 10 eV for the preedge region (8033−8303 eV), 0.5 eV for the edge region (8303−8363 eV), and a $k$-space interval of 0.05 Å$^{-1}$ for the EXAFS region (8366−9850 eV). Counting time per step was made for 1 s durations with a delay period of 0.3 s between successive data points in order for the monochromator to reach equilibrium. The energy calibration of the monochromator was monitored using a Ni foil employing a third ion chamber filled with the same gas as that of the transmitted beam ion chamber.

To minimize the effect of particle size on EXAFS amplitudes,[32] powdered samples were prepared by grinding and sieving through a 20 $\mu$m size nylon screen. For NiO the fine powder was then deposited on Kapton tape, and eight layers were stacked to give a relatively uniform thickness with an X-ray absorption edge jump, $\Delta\mu x$, of 1.12. For other oxide samples, a portion of the finely ground and sieved powder was mixed thoroughly with boron nitride and pressed into a pellet. The thickness of each pellet was sufficient to yield a $\Delta\mu x$ of 0.95, 0.68, 0.89, and 0.67 for $\beta$-Ni(OH)$_2$, $\alpha$-Ni(OH)$_2$, LiNiO$_2$, and KNiIO$_6$, respectively. A 4 $\mu$m thick Ni foil with a $\Delta\mu x$ of 1.07 was used as a standard for energy calibration. The X-ray

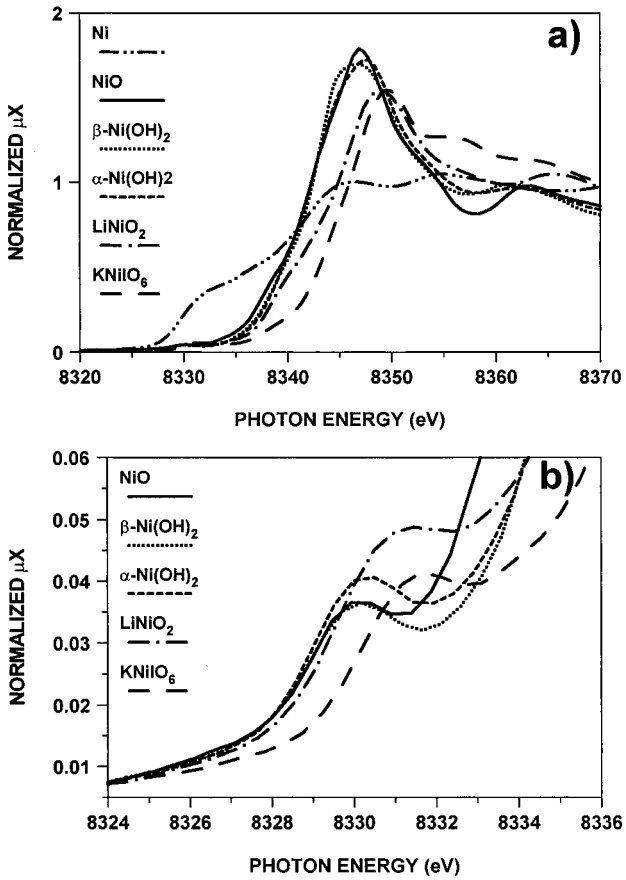


**Figure 1.** Normalized XANES of Ni K-edge (a) and Ni K-preedge structure (b) as a function of nickel Valency for metallic Ni, NiO, $\beta$-Ni(OH)$_2$, $\alpha$-Ni(OH)$_2$, LiNiO$_2$, and KNiIO$_6$.

absorption edge jump for each sample was kept below 1.5 in order to minimize the thickness effect.[33]

## Results and Discussion

The preedge background was determined from a quadratic fit to the data from about 300 to 30 eV below the edge energy and then extrapolating over the entire energy range of the spectrum. A few minor glitches, each extending over a narrow energy range, were present in the spectra. The glitch data were replaced by values obtained from a fourth-order polynomial fit to 10 data points adjacent to the glitch region with 5 data points selected on each side of the glitch. The EXAFS spectrum, $\chi(k)$, was extracted using cubic spline procedures which minimize the amplitude on nonphysical peaks in the low $r$-space region (0−1 Å) of the Fourier transform.[34−36] The photoelectron wavenumber was defined assuming an edge energy of 8333.0 eV (see Figure 1). An energy independent step normalization was then applied by dividing by the value of the atomic absorption at 100 eV above the edge energy. An energy dependent normalization was also applied to the $\chi(k)$ data using the normalized atomic absorption (also normalized at 100 eV above the edge energy) calculated with McMaster coefficients.[37]

**XANES Region.** Figure 1a shows the XANES spectra of the Ni K-edge as a function of nickel valency in NiO, $\beta$-Ni(OH)$_2$, $\alpha$-Ni(OH)$_2$, LiNiO$_2$, and KNiIO$_6$ along with that of metallic Ni used as a reference. The edge energies measured at half-height are listed in Table 2 and presented graphically in Figure 2a. As expected, the Ni K-edge shifts to higher energies as the oxidation state increases from Ni$^0$ (metallic Ni), to Ni$^{2+}$ (NiO and Ni(OH)$_2$), and Ni$^{4+}$ (KNiIO$_6$). The latter is among the few compounds where Ni has been established to be in the quadrivalent state[38] and was chosen here as a reference for Ni$^{4+}$ because of its stability and ease of preparation. The XANES spectrum for LiNiO$_2$ shows a shoulder at the onset of the edge similar to that for NiO, suggesting the presence of Ni$^{2+}$. Indeed, our EXAFS results (shown later in the text) show that approximately one-third of the Ni−O bonds are in the form of Ni$^{2+}$−O$^{2-}$. This is not surprising if one considers LiNiO$_2$ as Li-doped NiO.[39−41] The edge energy for LiNiO$_2$ is intermediate to those of NiO and KNiIO$_6$, suggesting that the oxidation state of Ni in LiNiO$_2$ is near 3. However, on the basis of oxygen K-edge X-ray absorption spectra,[42] X-ray photoemission spectroscopy, and bremsstrahlung isochromat spectroscopy,[43,44] as well as the Ni 2p X-ray absorption spectra[45−47] of LiNiO$_2$, it was concluded that the charge-compensating mechanism in LiNiO$_2$ was dominated by O 2p holes rather than the conventionally assumed Ni 3d holes of the NiO$_6$ cluster. Thus, the oxidation state of Ni in LiNiO$_2$ was assumed to be closer to 2 than 3. A similar situation was observed for Cu in high-temperature superconductors (HTS) such as YBa$_2$Cu$_3$O$_7$.[48,49]

**TABLE 2: Ni K-Edge Energies in Various Compounds**[a]

| compound | Ni K-edge energy (eV)[b] | Ni preedge peak energy (eV)[c] |
|---|---|---|
| Ni | 8336.7 | N/A |
| NiO | 8339.2 | 8328.7(8330.2) |
| $\beta$-Ni(OH)$_2$ | 8339.5 | 8328.7(8330.2) |
| $\alpha$-Ni(OH)$_2$ | 8339.5 | 8328.7(8330.4) |
| LiNiO$_2$ | 8340.6 | 8329.2(8331.6) |
| KNiIO$_6$ | 8342.9 | 8329.9(8331.7) |

[a] Energies are accurate to within ±0.1 eV. [b] Ni K-edge energy measured at half-height of the edge step. [c] Ni K-edge energy measured at half-height of the preedge peak intensity. Energies in parentheses correspond to the preedge peak energy.

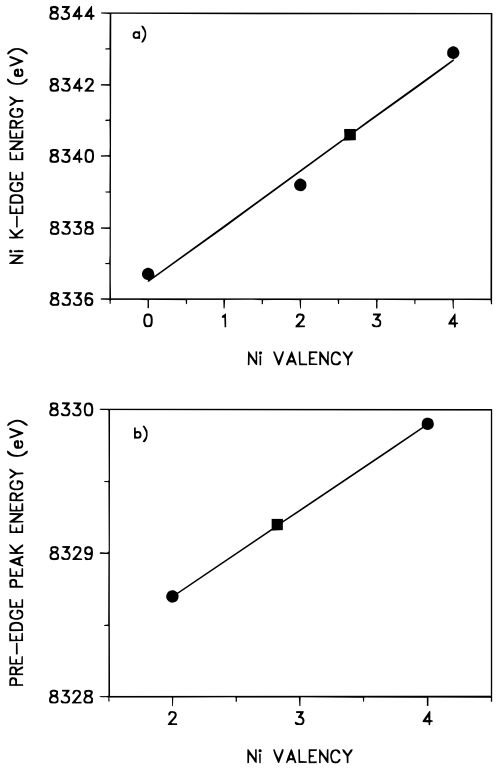


**Figure 2.** X-ray Absorption Ni K-edge energy (a) and Ni K-preedge energy (b) as a function of nickel valency. The solid curves represent a linear fit optimized against the valency of Ni in LiNiO$_2$. The best fit yields a valency of 2.65 ± 0.07 from the main edge data (a) and a 2.82 ± 0.17 from the preedge data (b).

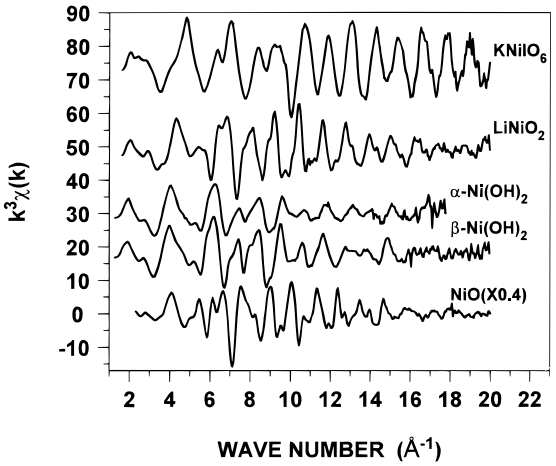


**Figure 3.** Normalized Ni K-edge EXAFS spectra, $k^3\chi(k)$, for NiO, $\beta$-Ni(OH)$_2$, $\alpha$-Ni(OH)$_2$, LiNiO$_2$, and KNiIO$_6$.

Assuming that the Ni K-edge energy is linearly proportional with nickel valency, as has been demonstrated by many authors, an optimum fit yields an average oxidation state for Ni in LiNiO$_2$ of 2.65 $\pm$ 0.07, as shown by the square symbol in Figure 2a.

The preedge peak, which is due to the transition from the 1s core level to bound unoccupied d states near the Fermi level, is shown in Figure 1b. The weak intensity (3−5%) associated with this transition is due to the fact that this transition is forbidden by dipole selection rules. It is allowed by quadrupole selection rules or as a result of hybridization between unoccupied states with p and d character. The occupancy of d states depends strongly on the chemical environment, local structure, and site symmetry, and hence, the signature of d states in the XANES is expected to vary with changes in Ni valency. The preedge peak energies at half-height as well as the preedge peak energies are listed in Table 2. Similar to the main edge energies, the preedge peak energy at half-height (Figure 2b) shifts to higher energy with increase in valency of Ni from $Ni^{2+}$ (NiO) to $Ni^{4+}$ ($KNiIO_6$) with that of $LiNiO_2$ being intermediate to those of $Ni^{2+}$ and $Ni^{4+}$. On the basis of linear interpolation using the preedge peak energies for NiO and KNiIO$_6$, the average valency of Ni in LiNiO$_2$ is estimated to be 2.82 $\pm$ 0.17, as shown by the square symbol in Figure 2b. This estimate is in agreement with the estimate of 2.65 $\pm$ 0.07 based on the main edge energies. The Ni valency in LiNiO$_2$ will be discussed later in the text in the context of the EXAFS results. Note that both NiO and KNiIO$_6$ display sharp preedge peaks that are significantly narrower than those of $\beta$- and $\alpha$-Ni(OH)$_2$. It is also seen that while both $\beta$- and $\alpha$-Ni(OH)$_2$ display well-defined preedge peaks, the intensity of the preedge peak for $\alpha$-Ni(OH)$_2$ is greater than that for $\beta$-Ni(OH)$_2$, which may be due to a smaller Ni−O bond length and/or a higher degree of structural disorder for $\alpha$-Ni(OH)$_2$ compared to that for $\beta$-Ni(OH)$_2$; these can enhance hybridization between O 2p and Ni 3d states, resulting in an increased intensity of the preedge peak.

**EXAFS Region.** A comparison of the normalized Ni K-edge EXAFS data, $k^3\chi(k)$, for NiO, $\beta$-Ni(OH)$_2$, $\alpha$-Ni(OH)$_2$, LiNiO$_2$, and KNiIO$_6$ and their corresponding phase-uncorrected Fourier transforms are shown in Figures 3 and 4, respectively. Note that the $k^3\chi(k)$ spectra and their corresponding Fourier transforms have been shifted vertically relative to that of NiO for clarity of presentation and that the $k^3\chi(k)$ spectrum for NiO and its corresponding Fourier transform were scaled vertically by a factor of 0.4. The Fourier transforms were performed using the $k$-space ranges ($k_{min}$−$k_{max}$) of 1.7−16.9, 1.6−16.3, 1.5−16.1, 1.8−16.1, and 1.8−16.4 Å$^{-1}$ for NiO, $\beta$-Ni(OH)$_2$, $\alpha$-Ni(OH)$_2$, LiNiO$_2$, and KNiIO$_6$, respectively, without applying a hanning window. A hanning window was not necessary since $k_{min}$ and $k_{max}$ were chosen such that $\chi(k_{min})=\chi(k_{max}) = 0$. It is evident from Figures 3 and 4 that the EXAFS spectrum for $\beta$-Ni(OH)$_2$ resembles closely that of $\alpha$-Ni(OH)$_2$. The spectra for NiO, LiNiO$_2$, and KNiIO$_6$ are quite distinct from each other and also from those of $\beta$-Ni(OH)$_2$ and $\alpha$-Ni(OH)$_2$, reflecting differences in the local structure of nickel in these phases. The Fourier transforms for NiO and LiNiO$_2$ display several well-defined peaks corresponding to contributions from the first few coordination spheres, which are indicative of the highly crystalline nature of these phases. The Fourier transform for LiNiO$_2$ is qualitatively similar to that of NiO except for variations due to the low backscattering amplitude of lithium atoms compared to that of nickel atoms and different ionic radii of nickel due to change in nickel valency. For example, the position of the first peak in the Fourier transform for LiNiO$_2$ is shifted to a lower distance relative to that of NiO due to the greater valency of Ni in LiNiO$_2$. The second peak in the Fourier transform for LiNiO$_2$, with a contribution mainly from six Ni atoms at 2.88 Å and a minor contribution (negligible) from six Li atoms at 2.89 Å, has an amplitude per nickel atom that is similar to the amplitude per nickel atom derived from the second peak in the Fourier transform for NiO which originates from 12 Ni atoms at 2.95 Å. The third peak in the Fourier transform for NiO, which corresponds to the fourth coordination sphere containing six Ni atoms at 4.18 Å, is absent from the Fourier transform for LiNiO$_2$ due to the fact that the atoms contributing to this peak are now Li atoms, which have significantly reduced backscattering amplitudes. The Fourier transform for KNiIO$_6$ displays several peaks characteristic of the highly crystalline nature of this material. The first peak corresponds to Ni−O interactions, and its position is slightly shifted to a lower distance relative to that of LiNiO$_2$. The second peak corresponds to Ni−I interactions with a small contribution from six oxygen atoms at 3.55 Å as will be shown later in the text.

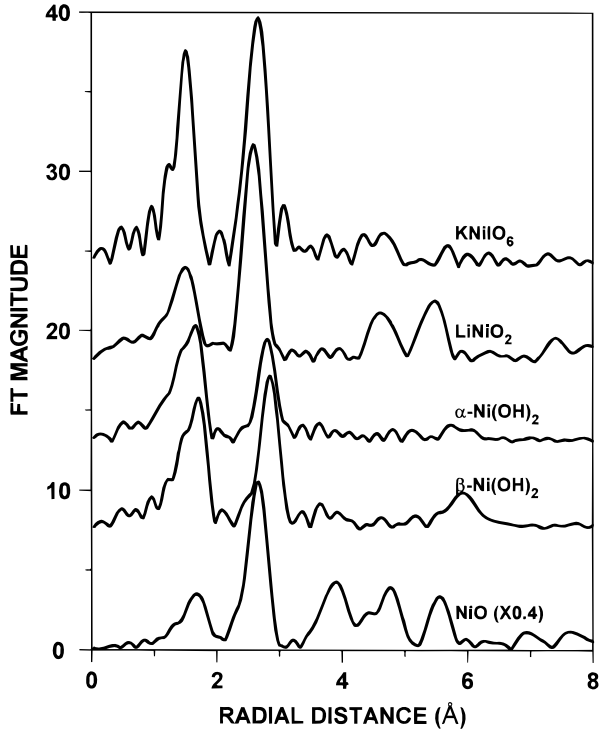


**Figure 4.** Fourier transforms of normalized Ni K-edge EXAFS spectra $k^3\chi(k)$ for NiO, $\beta$-Ni(OH)$_2$, $\alpha$-Ni(OH)$_2$, LiNiO$_2$, and KNiIO$_6$.

The Fourier transforms of $\beta$-Ni(OH)$_2$ and $\alpha$-Ni(OH)$_2$ are consistent with the brucite C6 type structure, which is a layered structure consisting of nickel hexagonal planes with $OH^-$ groups sandwiched between the planes. The Fourier transforms for $\beta$-Ni(OH)$_2$ and $\alpha$-Ni(OH)$_2$ each show three distinct peaks. The first peak corresponds to Ni−O interactions resulting from the octahedral coordination of Ni with oxygen. The second and third peaks, located at about 2.8 and 5.9 Å, correspond to Ni−Ni interactions from within the same hexagonal plane. The absence of a peak at roughly 4.3 Å (in the phase-uncorrected Fourier transform), corresponding to the crystallographic distance of the interplanar separation of 4.6−4.7 Å, indicates a high degree of structural disorder between the planes. It is also worth noting that the intensities of the second and third peaks in the Fourier transform for $\alpha$-Ni(OH)$_2$ are significantly smaller than those for $\beta$-Ni(OH)$_2$, indicating a higher degree of structural disorder within the hexagonal planes for $\alpha$-Ni(OH)$_2$ relative to that for $\beta$-Ni(OH)$_2$.

Quantitative analyses were made as follows. For each sample, except for metallic Ni, three different sets of filtered EXAFS data were generated. These were $\chi_1(k)$, $\chi_2(k)$, and $\chi_{1,2}(k)$, which include contributions from the first, second, and the combined contributions from the first and second peaks in the Fourier transform, respectively. For metallic Ni, only the filtered $\chi_1(k)$ data were generated. The *r*-space ranges used to generate the filtered $\chi_1(k)$ data were 1.14−2.80, 0.56−2.12, 0.54−2.14, 0.54−2.10, 0.70−2.04, and 0.50−2.20 Å for Ni, NiO, $\beta$-Ni(OH)$_2$, $\alpha$-Ni(OH)$_2$, $LiNiO_2$, and $KNiIO_6$, respectively. Those used to generate the filtered $\chi_2(k)$ data were 2.12−3.32, 2.15−3.50, 2.10−3.36, 2.04−3.04, and 2.02−3.36 Å for NiO, $\beta$-Ni(OH)$_2$, $\alpha$-Ni(OH)$_2$, $LiNiO_2$, and $KNiIO_6$, respectively. The windows utilized in generating the $\chi_1(k)$ and $\chi_2(k)$ data were combined to generate the filtered $\chi_{1,2}(k)$ data. The filtered data are related to local structure parameters in the framework of the cumulant expansion method[50] according to

$$\chi(k) = -\sum_i \frac{S_0^2 N_i}{kR_i^2} a(k) \times F_i(\pi,k,R) e^{-2(R_i/\lambda(k))} e^{-2\sigma_i^2 k^2 + (2/3)C_{4i}k^4} \times \sin\left(2R_i k - \frac{4}{3}C_{3i}k^3 + 2\delta(k) + \phi_i(k)\right)$$

where $N_i$ is the number of atoms of the *i*th type at distance $R_i$. The $\sigma_i^2$ is the disorder (i.e., mean squared relative displacement about the average distance $R_i$). The second term in the phase, $C_{3i}k^3$, accounts for phase changes due to non-Gaussian disorder. The term, $C_{4i}k^4$, was added to the EXAFS Debye−Waller factor to also account for non-Gaussian disorder. The terms $\delta(k)$ and $\phi(k)$ represent modifications in the phase shift of the ejected photoelectron wave function by the potential of the central absorbing and backscattering atoms, respectively. The other terms $\lambda(k)$, $F_i(\pi,k,R)$, and $a(k)$ represent the electron mean free path, the magnitude of the effective curved-wave backscattering amplitude for the *i*th type of atoms, and intrinsic losses as well as final state interference effects, respectively. The many-body amplitude reduction factor, $S_0^2$, is an energy independent term that accounts for losses only within the central absorbing atom.

Theoretical standards based on the curved-wave scattering formalism were utilized in fitting the data. Specifically, the $a(k)$, $\lambda(k)$, $\delta(k)$, $\phi(k)$, and $F(\pi,k,R)$ values were determined with the FEFF code[51,52] (version 5) using structural data listed in Table 1. The information needed to perform the calculations are the type of atoms and the coordinates for each atom in the cluster. For each cluster we have included information for all shells up to a radius of nearly 6 Å. The code uses a relativistic Dirac−Fock−Slater Desclaus atom code with the von Barth−Hedin ground-state exchange correlation potential. Scattering states were calculated using overlapped atom potentials and the complex Hedin−Lundquist potential to describe the exchange and correlation effects for excited states. The muffin-tin radii were calculated from the Norman radii. The natural broadening for the nickel edge was taken to be 1.6 eV. Examination of theoretical backscattering amplitudes for hydrogen, oxygen, and nickel in $\beta$-Ni(OH)$_2$ and for lithium, oxygen, and nickel in $LiNiO_2$ show that the backscattering amplitudes for hydrogen and lithium are significantly smaller than those of oxygen or nickel atoms. Hence, the hydrogen and lithium contributions to the EXAFS spectra were ignored.

All multiple scattering (MS) paths within the analyzed region were examined in detail. All MS paths were found to be of the nonfocusing type with amplitudes that are small enough and will not make a significant contribution to the XAFS spectra. Hence, their contributions were completely neglected. For metallic nickel, the first MS path is a three-leg path with an effective radius of 3.74 Å, which is well outside the *r*-space range of the first coordination sphere considered for analysis here. For NiO, two three-leg (O−O−Ni and Ni−O−Ni) MS paths with an effective radius of 3.57 Å have small contributions and were ignored. These two multiple scattering paths are well outside the *r*-space range of the first and second coordination spheres of oxygen and nickel atoms but are in close proximity of the third coordination sphere of oxygen atoms. The sum of the amplitudes for these two MS paths is significantly smaller than the amplitude of the single scattering (SS) contribution of the first and second coordination spheres. The sum of their amplitudes is even slightly lower than the SS contribution of the third shell of oxygen atoms, which is in itself much smaller than the SS scattering contributions of the first and second coordination spheres. Taking into account that MS contributions have higher effective disorders than SS contributions, MS contributions to the EXAFS spectra are further reduced. For $\beta$-Ni(OH)$_2$, two three-leg (H−O−Ni and O−O−Ni) MS paths with effective radii of 2.97 and 3.46 Å, respectively, had amplitudes comparable to the SS contribution of the second coordination sphere of hydrogen atoms. Since, even the SS contribution of hydrogen atoms is significantly smaller than the SS contributions of oxygen and nickel atoms and cannot be resolved from the experimental spectra, the MS contributions are also small and can be ignored. Similar arguments can be made for $\alpha$-Ni(OH)$_2$. For $LiNiO_2$, four three-leg (O−O−Ni, O−O−Ni, Ni−O−Ni, and Li−O−Ni) MS paths all with an effective radius of 3.49 Å, respectively, were examined. All are relatively outside the analyzed region, with amplitudes that are smaller than the SS scattering contribution of the third coordination sphere of lithium atoms. The SS contribution of the lithium sphere is much smaller than the SS contribution of the first coordination sphere of oxygen atoms or the second coordination sphere of nickel atoms and cannot be resolved from the experimental spectra. Hence, the contribution of these MS paths can also be ignored. For $KNiIO_6$, a three-leg (I−O−Ni) MS path with an effective radius of 3.61 Å has an amplitude that is only 7% that of the SS path of the first coordination sphere and was neglected. This MS path is in close proximity to the SS path of the third shell of oxygen atoms and has an amplitude that is roughly 20% that of the SS amplitude of the third shell of oxygen atoms. As mentioned above, since MS

**TABLE 3: Local Structure Parameters for Metallic Nickel[a]**

| filtered data | W | X-Y pair | $S_0^2$ | N | R (Å) | δR (Å) | $\sigma^2$ ($10^{-3}$ Å$^2$) | $\Delta E_0$ (eV) | SSR |
|---|---|---|---|---|---|---|---|---|---|
| $\chi_1$ | 3 | Ni−Ni | 0.78 | 12 | 2.478 | −0.014 | 5.5 | −2.7 | 5.9 |
| | 2 | Ni−Ni | 0.77 | 12 | 2.479 | −0.013 | 5.4 | −2.9 | 0.13 |
| | 1 | Ni−Ni | 0.75 | 12 | 2.480 | −0.012 | 5.2 | −3.0 | 0.004 |

[a] *N*: coordination number. *R*: coordination distance. $\sigma^2$: mean square relative displacement. $\Delta E_0$: inner potential correction. *W*: *k*-weighting exponent. SSR: sum of the square of residuals between experimental and calculated spectra. Fits were performed using theoretical standards generated from structure data for metallic nickel (see Table 1). $\delta R = R$(EXAFS) − $R$(XRD). All fits were refined over the *k*-range 4−16 Å$^{-1}$.

paths have higher effective disorders, their contributions to the EXAFS spectra are further reduced.

Since the information content of the EXAFS data is bandwidth limited, the maximum number of fit parameters was kept less than or equal to the number of independent data points, $N_{idp}$, given by the formula $N_{idp} = 2\Delta k\Delta R/\pi + 2$, where $\Delta k$ is the *k*-space range over which $\chi(k)$ is fitted and $\Delta R$ is the filtered *r*-space range.[53−55] In fitting the filtered EXAFS spectra with eq 1, a Gaussian disorder was initially assumed. Hence, the third and fourth cumulant terms were both set equal to zero, and only four parameters per shell are usually varied: $N$, $R$, $\sigma$,$^2$ and an inner potential energy shift ($\Delta E_0$) used in the final definition of the photoelectron wavenumber *k*. However, when theoretical standards generated with the FEFF code are used, a fifth parameter is introduced, namely, the energy independent many-body amplitude reduction factor $S_0^2$. Hence, only the product of $S_0^2$ and $N$ could be determined unless the value of either one was known a priori. In this study, the coordination numbers for all of the compounds investigated are well-known, and hence, we have constrained $N$ to its crystallographic value and used $S_0^2$ as a fitting parameter. A single-shell fit was sufficient to satisfactorily model the filtered $\chi_1(k)$ and $\chi_2(k)$ for all of the compounds investigated here except in the case of $\chi_1(k)$ for $LiNiO_2$ and $\chi_2(k)$ for NiO and $KNiIO_6$, where a two-shell fit was required to correctly model the experimental data. Consequently, assuming a Gaussian disorder, four floating parameters ($S_0^2$, R, $\sigma$,$^2$ and $\Delta E_0$) were employed in the case of the single-shell fit analysis. The only exceptions were in analyzing the contributions of the third coordination sphere of oxygen atoms for NiO and the third coordination sphere of nickel atoms for α-$Ni(OH)_2$, where single-shell fits with four, five, and six floating parameters were employed. The five- and six-parameter fits included the third cumulant expansion term ($C_3$) and the third as well as the fourth cumulant expansion terms ($C_3$ and $C_4$), respectively, which were used to account for non-Gaussian disorder. The $\chi_1(k)$ for $LiNiO_2$ required a two-shell fit with both Ni−O contributions to correctly model the experimental data. Furthermore, the filtered $\chi_2(k)$ for NiO and $KNiIO_6$ each required a two-shell fit composed of one shell of Ni−Ni (for NiO) or Ni−I (for $KNiIO_6$) and one shell of Ni−O contributions. Fits were performed in the *k*-ranges of 4−16 Å$^{-1}$ (nickel) and 4−14 Å$^{-1}$ (other samples). We discuss here the results for each sample.

**Ni.** Analysis for metallic Ni is limited to the first coordination sphere. Analysis of higher coordination spheres is complicated by multiple scattering effects, which are beyond the scope of this paper. Results of single-shell fit analysis as a function of *k*-weighting exponent ($W$) are listed in Table 3. Our results as a function of the *k*-weighting exponent for the room-temperature data show that the value of $S_0^2$ is in the range 0.75−0.78. It is worth pointing out that the value of $S_0^2$ increased with decrease in temperature and had a value of 0.84 when it was determined from EXAFS data measured at a temperature of 50 K. This should not be taken to indicate that the value of $S_0^2$ is temperature dependent. It may be an artifact of our analysis procedure, which assumed a Gaussian model for thermal disorder throughout the temperature range 50−300 K. This range of values is consistent with an earlier result which gave a value of 0.82 obtained by Li et al.[56] from Ni EXAFS measured at 83 K. The first-shell distance is slightly shorter than the crystallographic distance by 0.012−0.014 Å, which is generally the case for many compounds analyzed using theoretical standards. This value should be treated as a correction factor to be applied to distances determined for compounds with unknown structures. The disorder of 0.0052−0.0055 Å$^2$ for the Ni−Ni atom pair is consistent with results calculated using the correlated Debye model using FEFF5. Using $\theta(0\text{ K}) = 427$ K[57] yields a disorder of 0.005 49 Å$^2$, which is in excellent agreement with the experimental value. Recent work[58] showed that disorders for metallic Ni, calculated using $\theta(0\text{ K}) = 427$ K, are in excellent agreement with the experimentally determined disorders in the temperature range 50−300 K.

**NiO.** Analysis for NiO was made using theoretical standards generated with structure data for both NiO and β-$Ni(OH)_2$. Results are summarized in Table 4. A single-shell fit to the filtered $\chi_1(k)$ using theoretical standards generated from structure data for NiO yielded an $S_0^2$ value in the range 0.67−0.74 for *k*-weighting of 1, 2, and 3. A single-shell fit with a *k*-weighting of 3 using theoretical standards generated from structure data for β-$Ni(OH)_2$ yielded an $S_0^2$ value of 0.72 compared to 0.74 when NiO theoretical standards are used. The local structure results are essentially the same regardless of whether theoretical standards based on structure data for NiO or β-$Ni(OH)_2$ are used. The average distance for the first shell is 2.074 Å, which is slightly shorter than the crystallographic distance by 0.015 Å. The disorder for the first shell of the Ni−O atom pair is in the range 0.0024−0.0035 Å$^2$ for *k*-weighting of 1, 2, and 3. A $k^3$-weighted single-shell fit to the filtered $\chi_2(k)$ using Ni−Ni theoretical standards yielded an $S_0^2$ value of 0.94. This fit is significantly improved with a two-shell fit which includes the contribution from the eight oxygen atoms of the third coordination sphere. The sum of the square of residuals (SSR) for the two-shell fit is smaller than that for the single-shell fit by a factor of 5. As pointed out by Haskel et al.,[59] a separate $\Delta E_0$ must be used for each type of backscattering atom, and hence, two $\Delta E_0$ were used as floating parameters: one for Ni−Ni and the other for Ni−O. The $k^3$-weighted two-shell fit yields a many-body amplitude reduction factor, $S_0^2$, of 0.89. The second-shell distance of 2.949 Å is slightly shorter than the crystallographic distance of 2.954 Å. However, the third-shell distance of 3.454 Å is significantly smaller than the crystallographic distance of 3.617 Å. The third-shell distance also shows significant dependence on the degree of the *k*-weighting of the data, with results from the *k*-weighted fit being closer to the crystallographic value than that obtained from the $k^3$-weighted fit. The third-shell distance obtained from the *k*-weighted fit is 3.531 Å; this distance is still significantly smaller than the crystallographic value by 0.086 Å. Inconsistent results for the third-shell of NiO were also obtained by Kuzmin et al.[60] using the FEFF3 code and a Gaussian pair distribution function. To examine if this discrepancy in the distance of the third shell of oxygen atoms is due to an asymmetric pair distribution function (PDF), we have performed two-shell fits utilizing (i) the third cumulant term, $C_3$, and (ii) the third and fourth cumulant terms, $C_3$ and $C_4$, as floating parameters. A

**TABLE 4: Local Structure Parameters for NiO[a]**

| filtered data and model | *W* | X-Y pair | $S_0^2$ | *N* | *R* (Å) | $\delta R$ (Å) | $\sigma^2$ ($10^{-3}$ Å$^2$) | $C_3$ ($10^{-4}$ Å$^3$) | $C_4$ ($10^{-5}$ Å$^4$) | $\Delta E_0$ (eV) | SSR |
|---|---|---|---|---|---|---|---|---|---|---|---|
| $\chi_1$, M1 | 3 | Ni−O | 0.74 | 6 | 2.078 | −0.011 | 3.5 | | | −8.4 | 19.7 |
| | 2 | Ni−O | 0.67 | 6 | 2.074 | −0.016 | 3.0 | | | −7.9 | 0.34 |
| | 1 | Ni−O | 0.67 | 6 | 2.070 | −0.019 | 2.4 | | | −7.3 | 0.007 |
| $\chi_1$, M2 | 3 | Ni−O | 0.72 | 6 | 2.077 | −0.012 | 3.4 | | | −8.3 | 20.6 |
| $\chi_2$, M1 | 3 | Ni−Ni | 0.91 | 12 | 2.945 | −0.009 | 5.5 | | | −5.3 | 93.5 |
| $\chi_2$, M1 | 3 | Ni−Ni | 0.89 | 12 | 2.949 | −0.005 | 5.4 | | | −6.4 | 18.1 |
| | | Ni−O | | 8 | 3.454 | −0.163 | 9.3 | | | −1.8 | |
| | 3 | Ni−Ni | 0.95 | 12 | 2.955 | +0.001 | 5.7 | | | −7.3 | 10.9 |
| | | Ni−O | | 8 | 3.562 | −0.055 | 5.4 | 15.6 | | −5.0 | |
| | 3 | Ni−Ni | 0.99 | 12 | 2.952 | −0.003 | 6.2 | | | −6.5 | 5.4 |
| | | Ni−O | | 8 | 3.615 | −0.002 | 12.8 | 16.8 | 17.9 | −8.6 | |
| $\chi_{1,2}$, M1 | 3 | Ni−O | 0.87 | 6 | 2.071 | −0.017 | 5.0 | | | −6.3 | 35.7 |
| | | Ni−Ni | | 12 | 2.946 | −0.008 | 5.3 | | | −5.6 | |
| | | Ni−O | | 8 | 3.510 | −0.107 | 13.5 | | | −6.3 | |
| | 3 | Ni−O | 0.87 | 6 | 2.074 | −0.015 | 4.9 | | | −7.0 | 22.9 |
| | | Ni−Ni | | 12 | 2.947 | −0.007 | 5.0 | | | −6.3 | |
| | | Ni−O | | 8 | 3.609 | −0.008 | 4.7 | 31.6 | | −7.0 | |
| | 3 | Ni−O | 0.86 | 6 | 2.075 | −0.014 | 4.9 | | | −7.0 | 22.3 |
| | | Ni−Ni | | 12 | 2.945 | −0.009 | 5.0 | | | −6.0 | |
| | | Ni−O | | 8 | 3.603 | −0.014 | 6.6 | 31.3 | 5.0 | −7.0 | |

[a] *N*: coordination number. *R*: coordination distance. $\sigma^2$: mean square relative displacement. $\Delta E_0$: inner potential correction. *W*: *k*-weighting exponent. SSR: sum of the square of residuals between experimental and calculated spectra. Fits were performed using theoretical standards generated from structure data for NiO (model M1) and $\beta$-Ni(OH)$_2$ (model M2) (see Table 1). $\delta R = R$(EXAFS) − $R$(XRD). All fits were refined over the *k*-range 4−14 Å$^{-1}$.

**TABLE 5: Local Structure Parameters for $\beta$-Ni(OH)$_2$[a]**

| filtered data | *W* | X-Y pair | $S_0^2$ | *N* | *R* (Å) | $\delta R^a$ (Å) | $\delta R^b$ (Å) | $\delta R^c$ (Å) | $\sigma^2$ ($10^{-3}$ Å$^2$) | $\Delta E_0$ (eV) | SSR |
|---|---|---|---|---|---|---|---|---|---|---|---|
| $\chi_1$ | 3 | Ni−O | 0.70 | 6 | 2.064 | −0.009 | −0.016 | −0.077 | 4.5 | −7.9 | 8.5 |
| | 2 | Ni−O | 0.70 | 6 | 2.066 | −0.007 | −0.014 | −0.075 | 4.5 | −8.4 | 0.15 |
| | 1 | Ni−O | 0.69 | 6 | 2.071 | −0.002 | −0.009 | −0.070 | 4.5 | −8.9 | 0.003 |
| $\chi_2$ | 3 | Ni−Ni | 0.83 | 6 | 3.128 | +0.002 | +0.007 | +0.007 | 6.3 | −7.1 | 6.9 |
| | 2 | Ni−Ni | 0.84 | 6 | 3.130 | +0.004 | +0.011 | +0.004 | 6.4 | −7.4 | 0.17 |
| | 1 | Ni−Ni | 0.88 | 6 | 3.132 | +0.006 | +0.013 | +0.006 | 6.9 | −7.6 | 0.007 |
| $\chi_{1,2}$ | 3 | Ni−O | 0.76 | 6 | 2.059 | −0.014 | −0.021 | −0.082 | 5.1 | −6.7 | 13.4 |
| | | Ni−Ni | | 6 | 3.127 | +0.001 | +0.008 | +0.001 | 5.9 | −6.8 | |
| | 2 | Ni−O | 0.75 | 6 | 2.059 | −0.014 | −0.021 | −0.082 | 5.2 | −6.9 | 0.28 |
| | | Ni−Ni | | 6 | 3.127 | +0.001 | +0.008 | +0.001 | 5.7 | −6.8 | |
| | 1 | Ni−O | 0.77 | 6 | 2.059 | −0.014 | −0.021 | −0.082 | 5.8 | −6.9 | 0.009 |
| | | Ni−Ni | | 6 | 3.126 | +0.000 | +0.007 | +0.000 | 5.7 | −6.7 | |

[a] *N*: coordination number. *R*: coordination distance. $\sigma^2$: mean square relative displacement. $\Delta E_0$: inner potential correction. *W*:*k*-weighting exponent. SSR: sum of the square of residuals between experimental and calculated spectra. Fits were performed using theoretical standards generated from structure data for $\beta$-Ni(OH)$_2$ (see Table 1). $\delta R^a = R$(EXAFS) − $R$(neutron diffraction) for $\beta$-Ni(OD)$_2$, $\delta R^b = R$(EXAFS) − $R$(neutron diffraction) for $\beta$-Ni(OH)$_2$, and $\delta R^c = R$(EXAFS) − $R$(XRD) for $\beta$-Ni(OH)$_2$. All fits were refined over the *k*-range 4−14 Å$^{-1}$.

two-shell fit which included the $C_3$ term as a floating parameter reduced the value of SSR by a factor of 2. Further improvement in the value of SSR (a factor of 2) was obtained when both $C_3$ and $C_4$ were included as floating parameters. The second- and third-shell distances of this fit are 2.952 and 3.615 Å, respectively. These distances are shorter than the crystallographic values by only 0.002 Å for each shell. The $S_0^2$ value of 0.99 obtained from fitting the filtered $\chi_2(k)$ data is, however, significantly greater than the value of 0.74 obtained from fitting the filtered $\chi_1(k)$ data using the $k^3$-weighted fit. To resolve this issue, we performed a fit to the filtered $\chi_{1,2}(k)$ data. This fit yielded an $S_0^2$ value of 0.86, which is intermediate to values obtained from fits to the filtered $\chi_1(k)$ and $\chi_2(k)$ data separately. This value of $S_0^2$ is much closer to that obtained for metallic Ni by Li et al.[56] and by us here.

Finally, we have found that the disorders for the Ni−O and Ni−Ni atom pairs cannot be reproduced with the correlated Debye model using a single Debye temperature. Instead, two Debye temperatures must be used: $\theta \approx 940$ K for the Ni−O first-shell disorder and $\theta \approx 470$ K for the Ni−Ni second-shell disorder.

***β*-Ni(OH)$_2$.** Analysis was made using theoretical standards generated with structure data for NiO and $\beta$-Ni(OH)$_2$. Results are essentially the same, and hence, only those based on $\beta$-Ni(OH)$_2$ are summarized in Table 5. Due to the low backscattering amplitude of hydrogen, contribution from the second coordination sphere, which consists of six hydrogen atoms, is negligible, and hence, reliable structure analysis for this shell of atoms is not possible. A single-shell fit to the filtered $\chi_1(k)$ data yields an $S_0^2$ value of 0.70, which is independent of the *k*-weighting exponent, compared to 0.85 (average value) obtained from fitting the filtered $\chi_2(k)$ data, which shows only a slight dependence on the *k*-weighting exponent. A fit to the filtered $\chi_{1,2}(k)$ data gives an intermediate value of 0.76 (average value), which is independent of the *k*-weighting exponent and is close to that obtained for metallic Ni. The Ni−O distance obtained from the single-shell or two-shell fit is clearly significantly shorter than the distance determined from the X-ray diffraction data but is in excellent agreement with the distance determined from neutron diffraction data. The Ni−Ni distance for the third coordination sphere is in agreement with the distance determined from either the X-ray or the neutron diffraction data. Hence, our results, which are based on analysis using theoretical standards as well as earlier results[8] based on

**TABLE 6: Local Structure Parameters for α-Ni(OH)$_2$[a]**

| filtered data | *W* | X-Y pair | $S_0^2$ | *N* | R (Å) | $\delta R$ (Å) | $\sigma^2$ ($10^{-3}$ Å$^2$) | $C_3$ ($10^{-4}$ Å$^3$) | $C_4$ ($10^{-5}$ Å$^4$) | $\Delta E_0$ (eV) | SSR |
|---|---|---|---|---|---|---|---|---|---|---|---|
| $\chi_1$ | 3 | Ni−O | 0.73 | 6 | 2.036 | −0.197 | 6.4 | | | −6.5 | 6.7 |
| | 2 | Ni−O | 0.73 | 6 | 2.038 | −0.195 | 6.4 | | | −6.8 | 0.11 |
| | 1 | Ni−O | 0.71 | 6 | 2.041 | −0.192 | 6.2 | | | −7.2 | 0.002 |
| $\chi_2$ | 3 | Ni−Ni | 0.66 | 6 | 3.092 | +0.009 | 8.3 | | | −6.6 | 18.1 |
| | 3 | Ni−Ni | 0.67 | 6 | 3.133 | +0.050 | 8.2 | 4.4 | | −9.7 | 12.9 |
| | 3 | Ni−Ni | 1.05 | 6 | 3.133 | +0.050 | 15.1 | 4.4 | 12.5 | −9.8 | 4.1 |
| $\chi_{1,2}$ | 3 | Ni−O | 0.77 | 6 | 2.031 | +0.202 | 6.9 | | | −5.3 | 10.6 |
| | | Ni−Ni | | 6 | 3.133 | +0.050 | 11.4 | 4.6 | 7.0 | −9.4 | |

[a] *N*: coordination number. *R*: coordination distance. $\sigma^2$: mean square relative displacement. $\Delta E_0$: inner potential correction. *W*:*k*-weighting exponent. SSR: sum of the square of residuals between experimental and calculated spectra. Fits were performed using theoretical standards generated from structure data for $\beta$-Ni(OH)$_2$ (see Table 1). $\delta R = R$(EXAFS) − $R$(idealized model for α-Ni(OH)$_2$) from ref 24. All fits were refined over the *k*-range 4−14 Å$^{-1}$.

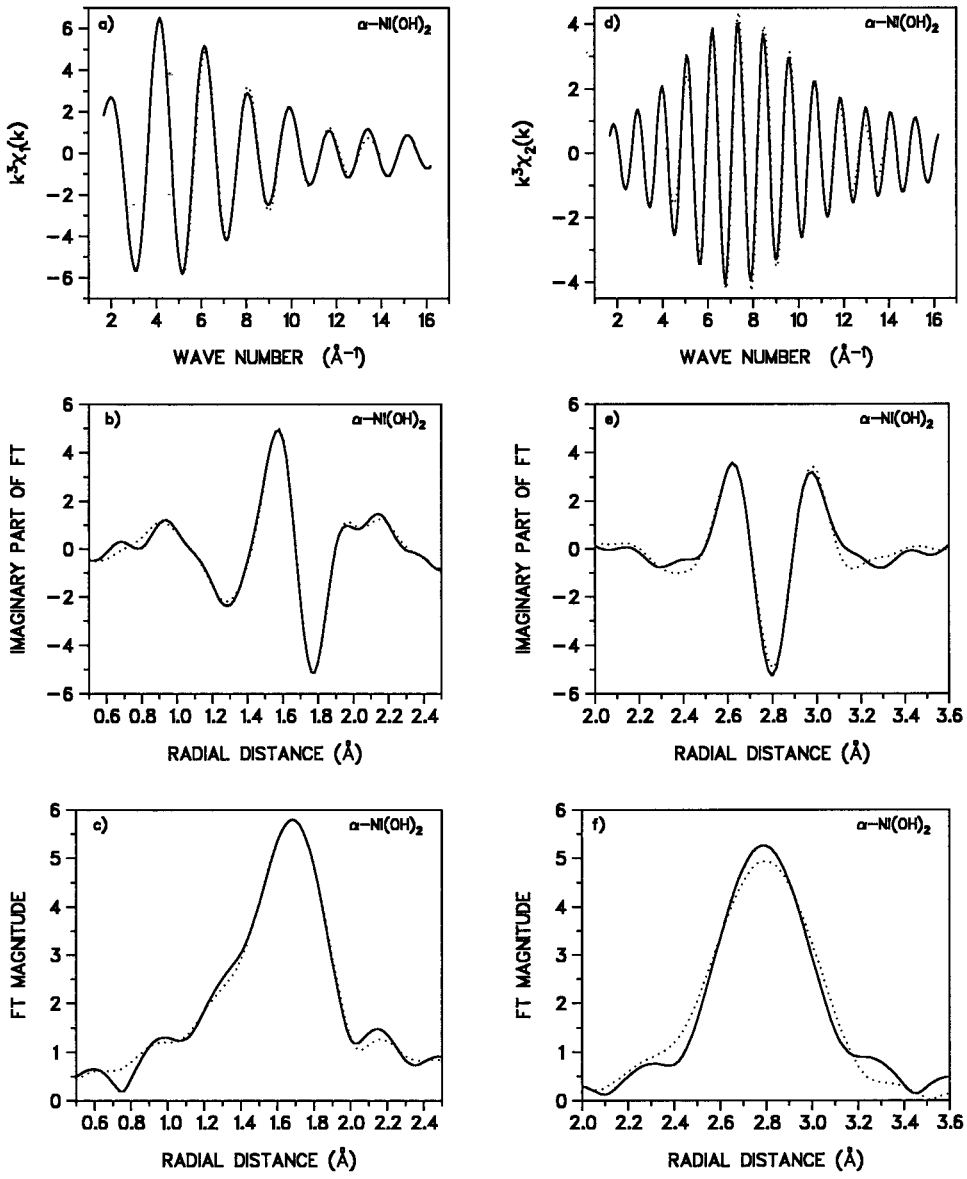


**Figure 5.** Experimental filtered data (solid curve) and calculated fit data (dotted curve) for α-Ni(OH)$_2$: a−c correspond to $k^3\chi_1(k)$, imaginary part of FT, and magnitude of FT, respectively, using one shell of Ni−O; d−f correspond to $k^3\chi_2$, imaginary part of FT, and magnitude of FT, respectively, using one shell of Ni−Ni.

empirical standards, show that the neutron diffraction data give an accurate description of the structure of both the oxygen and nickel atoms. Despite variations in the value of $S_0^2$ obtained from the various sets of filtered data, variations in the disorder are small. The Ni−O first-shell disorder is in the range 0.0045−0.0058 Å$^2$, while for the Ni−Ni third shell it is in the range 0.0057−0.0069 Å$^2$.

**α-Ni(OH)$_2$.** Analysis was made using theoretical standards generated with structure data for $\beta$-Ni(OH)$_2$. A summary of local structure parameters is listed in Table 6. Comparisons of calculated and experimental spectra are shown in Figures 5 and 6. As is the case for $\beta$-Ni(OH)$_2$, reliable structure analysis for the second coordination sphere, which consists of six hydrogen atoms, is not possible. A single-shell fit to the filtered $\chi_1(k)$

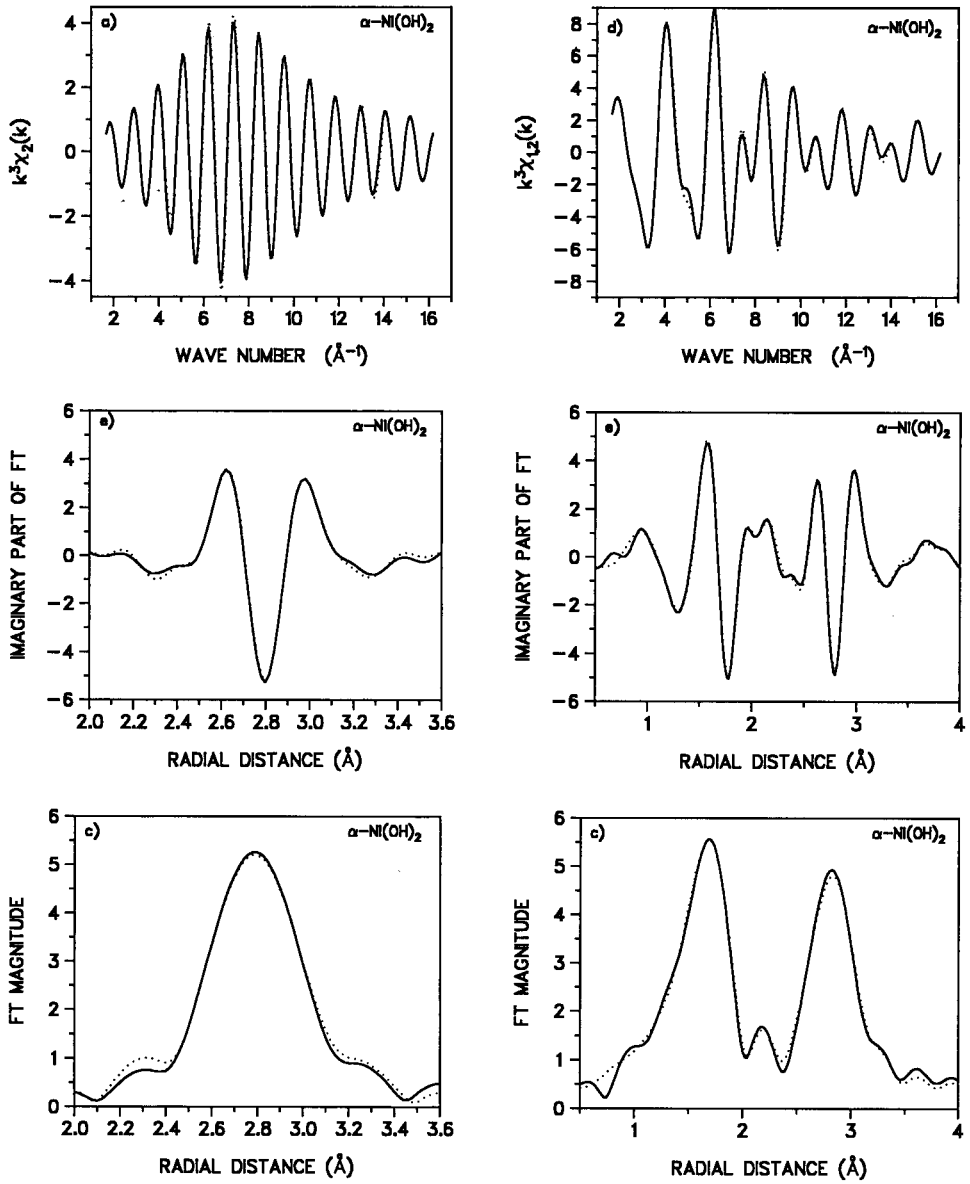


**Figure 6.** Experimental filtered data (solid curve) and calculated fit data (dotted curve) for α-Ni(OH)$_2$: a−c correspond to $k^3\chi_2$, imaginary part of FT, and magnitude of FT, respectively, using one shell of Ni−Ni with six parameters varied including $C_3$ and $C_4$ from the cumulant expansion; d−f correspond to $k^3\chi_{1,2}$, imaginary part of FT, and magnitude of FT, respectively, using one shell of Ni−O and one shell of Ni−Ni with six parameters varied (including $C_3$ and $C_4$ from the cumulant expansion) for the Ni−Ni contribution.

data using a Gaussian disorder yields an $S_0^2$ value of 0.73, which is independent of the *k*-weighting exponent. Comparisons of calculated and experimental spectra, shown in Figure 5 (a, b, and c) for a *k*-weighting of 3, indicate a high-quality fit. A single-shell fit to the filtered $\chi_2(k)$ data using a Gaussian disorder, on the other hand, gives a poor fit, as shown in Figure 5 (d, e, and f) for a *k*-weighting of 3. Results as a function of the *k*-weighting exponent (not shown here for *k*- and $k^2$-weighting) show $S_0^2$ values in the range 0.66−1.07, which should not be the case. Despite the poor quality of the fit, the Ni−Ni distance of 3.09 Å is in good agreement with the distance extracted based on the idealized structure model proposed by Bode et al. for α-Ni(OH)$_2$.[24] This distance, however, is shorter than that observed for $\beta$-Ni(OH)$_2$ by 0.04 Å. The contraction in the Ni−Ni distance for α-Ni(OH)$_2$ relative to that for $\beta$-Ni(OH)$_2$ is in agreement with an earlier result where a contraction of 0.05 Å was observed.[8] However, it was pointed out that the apparent distance contraction is not real but is due to disorder and particle size effects.[23] More recently, Pandya et al.[8] asserted that this distance contraction is real and is not due to structural disorder based on the facts that (i) the thermal vibrations are very small at 77 K, (ii) the distance contraction was temperature independent, and (iii) the distance was the same regardless of whether empirical standards used in the analysis were derived from NiO or $\beta$-Ni(OH)$_2$ data. In our opinion, all of these observations are not decisive in answering the question of whether the contraction is real or due to structural disorder. The first and second scenarios indicate that the contraction in the second-shell distance cannot be due to asymmetry because of thermal disorder. Since structural disorder is temperature independent (excluding the possibility of a phase transition which is not the case), it cannot be ruled out. The third observation merely shows that both NiO and $\beta$-Ni(OH)$_2$ are appropriate models for analyzing the local structure of α-Ni(OH)$_2$. However, accurate distance determination depends on using an accurate model for the disorder. Here, we provide evidence that the apparent contraction observed in the distance of the Ni−Ni third coordination sphere is not real. The quality of the single-shell fit to the filtered $\chi_2(k)$ data is significantly improved using an asymmetric instead of a Gaussian pair

**TABLE 7: Local Structure Parameters for $LiNiO_2$[a]**

| filtered data | $W$ | X-Y pair | $S_0^2$ | $N$ | $R$ (Å) | $\delta R$ (Å) | $\sigma^2$ ($10^{-3}$ Å$^2$) | $\Delta E_0$ (eV) | SSR |
|---|---|---|---|---|---|---|---|---|---|
| $\chi_1$ | 3 | Ni−O | 0.63 | 6 | 1.924 | | 8.1 | −5.9 | 21.2 |
| $\chi_1$ | 3 | Ni−O | 0.63 | 4 | 1.911 | | 3.7 | −9.0 | 8.4 |
| | | Ni−O | | 2 | 2.048 | | 3.7 | | |
| $\chi_2$ | 3 | Ni−Ni | 0.67 | 6 | 2.874 | −0.008 | 3.6 | −5.1 | 19.7 |
| | 2 | Ni−Ni | 0.71 | 6 | 2.875 | −0.007 | 4.0 | −5.4 | 0.67 |
| | 1 | Ni−Ni | 0.81 | 6 | 2.879 | −0.003 | 5.1 | −6.0 | 0.025 |
| $\chi_{1,2}$ | 3 | Ni−O | 0.66 | 3.8 | 1.901 | | 3.7 | −7.4 | 17.6 |
| | | Ni−O | | 2.2 | 2.038 | | 3.7 | −7.4 | |
| | | Ni−Ni | | 6 | 2.872 | −0.010 | 3.7 | −4.7 | |
| | 2 | Ni−O | 0.71 | 4.0 | 1.912 | | 4.7 | −8.2 | 0.38 |
| | | Ni−O | | 2.0 | 2.059 | | 4.7 | −8.2 | |
| | | Ni−Ni | | 6 | 2.871 | −0.011 | 4.0 | −4.5 | |
| | 1 | Ni−O | 0.79 | 4.3 | 1.931 | | 5.8 | −9.9 | 0.008 |
| | | Ni−O | | 1.7 | 2.106 | | 5.8 | −9.9 | |
| | | Ni−Ni | | 6 | 2.869 | −0.013 | 4.8 | −4.1 | |
| $\chi_{1,2}$ | 3 | Ni−O | 0.67 | 4 | 1.904 | | 4.0 | −7.3 | 17.6 |
| | | Ni−O | | 2 | 2.045 | | 3.3 | −7.3 | |
| | | Ni−Ni | | 6 | 2.872 | −0.010 | 3.7 | −4.7 | |
| | 2 | Ni−O | 0.71 | 4 | 1.912 | | 4.7 | −8.2 | 0.38 |
| | | Ni−O | | 2 | 2.058 | | 4.9 | −8.2 | |
| | | Ni−Ni | | 6 | 2.871 | −0.011 | 4.0 | −4.5 | |
| | 1 | Ni−O | 0.79 | 4 | 1.927 | | 5.4 | −10.0 | 0.008 |
| | | Ni−O | | 2 | 2.091 | | 7.1 | −10.0 | |
| | | Ni−Ni | | 6 | 2.869 | −0.013 | 4.8 | −4.1 | |

[a] $N$: coordination number. $R$: coordination distance. $\sigma^2$: mean square relative displacement. $\Delta E_0$: inner potential correction. $W$: $k$-weighting exponent. SSR: sum of the square of residuals between experimental and calculated spectra. Fits were performed using theoretical standards generated from structure for $LiNiO_2$. $\delta R = R$(EXAFS) − $R$(XRD). All fits were refined over the $k$-range 4−14 Å$^{-1}$.

distribution function. A five-parameter-single-shell fit which includes the third cumulant expansion term as a floating parameter reduces the sum of the square of residuals by a factor of 3, and a distance of 3.13 Å is obtained; this is the same as for $\beta$-$Ni(OH)_2$. Thus, the apparent contraction in the Ni−Ni distance can be explained by using an asymmetric pair distribution function to model disorder. Additional improvement in the quality of the fit is obtained with a six-parameter-single-shell fit which includes both the third and fourth cumulant expansion terms. Comparisons of calculated and experimental spectra shown in Figure 6 (a, b, and c) indicate the high quality of the fits. In this case, the sum of the square of residuals is reduced by a factor of 4.5 (Table 6), and the Ni−Ni distance is again the same as that for $\beta$-$Ni(OH)_2$. The sixth parameter fit, however, provides an $S_0^2$ value which is larger than that for metallic Ni due to the high degree of correlation between $S_0^2$, $\sigma$,[2] and $C_4$. This degree of correlation is reduced with a combined fit to the $\chi_{1,2}(k)$ data, which gives a many-body amplitude reduction factor of 0.76 for a $k$-weighting of 3 (Figure 6d,e,f). Small variations in the value of $S_0^2$ were obtained as a function of the $k$-weighting exponent. The single-shell fit to the filtered $\chi_1(k)$ data and the two-shell fit to the filtered $\chi_{1,2}(k)$ data give a Ni−O distance of 2.028−2.041 Å. Thus, the first-shell distance for α-$Ni(OH)_2$ appears to be shorter than that for $\beta$-$Ni(OH)_2$ by 0.02−0.04 Å. Whether the contraction in the Ni−O first-shell distance is real or due to structural disorder cannot be established in this case using the cumulant expansion method. The low backscattering amplitude for oxygen atoms at high $k$ values ($k$ > 8 Å$^{-1}$) reduces sensitivity to structural disorder which dominates in the high $k$-region of the spectrum. However, in light of the results for the Ni−Ni shell of atoms, the apparent Ni−O distance contraction is most likely due to structural disorder and is not real. The Ni−Ni distance of 3.13 Å is again similar to that obtained from the single-shell fit to the filtered $\chi_2(k)$ data. Despite variations in the value of $S_0^2$ obtained from the various sets of filtered data, variations in the disorder are small. The Ni−O first-shell disorder is in the range 0.0062−0.0089 Å$^2$, while that for the second shell is in the range 0.0082−0.0114 Å$^2$. These disorders are higher than those for $\beta$-$Ni(OH)_2$, indicating a high degree of structural disorder for α-$Ni(OH)_2$. The high degree of structural disorder is not surprising in light of the extremely weak intensities of its X-ray diffraction peaks and the large degree of hydration.

**$LiNiO_2$.** Analysis was made using theoretical standards generated with structure data for NiO and $LiNiO_2$. Both models yielded the same results, and hence, only those based on structure data for $LiNiO_2$ are summarized in Table 7. Comparisons of calculated and experimental spectra are shown in Figures 7 and 8. Due to the low backscattering amplitude of lithium, contributions from the third coordination sphere, which consists of six lithium atoms, were neglected. We have found that a single-shell fit to the filtered $\chi_1(k)$ data is not sufficient to model the structure of the first coordination sphere of the Ni−O atom pair, as evidenced by the poor quality of the fit shown in Figure 7 (a, b, and c). The quality of the fit is significantly improved with a two-shell fit. In this fit, the sum of the coordination numbers for the two subshells was constrained to be equal to 6, and all atoms were assumed to have the same disorder. An optimum fit (see Figure 7d,e,f) was obtained when $N_1$ and $N_2$ were set equal to 4 and 2, respectively, yielding distances of 1.91 and 2.05 Å. A fit in which the disorder for each subshell of atoms was used as a floating parameter yielded disorders that were too small to be physically meaningful. A single-shell fit to the filtered $\chi_2(k)$ data, on the other hand, is sufficient to analyze the structure of the second coordination sphere. It yielded a distance of 2.88 Å, which is in agreement with distance determined from the X-ray diffraction data. The single-shell fit to the filtered $\chi_2(k)$ gave an $S_0^2$ value in the range 0.66−0.81 for $k$-weighting exponents from 3 to 1. The local structure was also obtained from a fit to the filtered $\chi_{1,2}(k)$ data. In this case, a three-shell fit with two shells accounting for oxygen backscatterers and one shell accounting for nickel backscatterers was performed. Initially, we assumed that all oxygen atoms have the same disorder and used $N_1$ and $N_2$ for the two subshells of oxygen atoms as floating parameters, but with their sum being constrained to be equal to 6. $N_3$ for

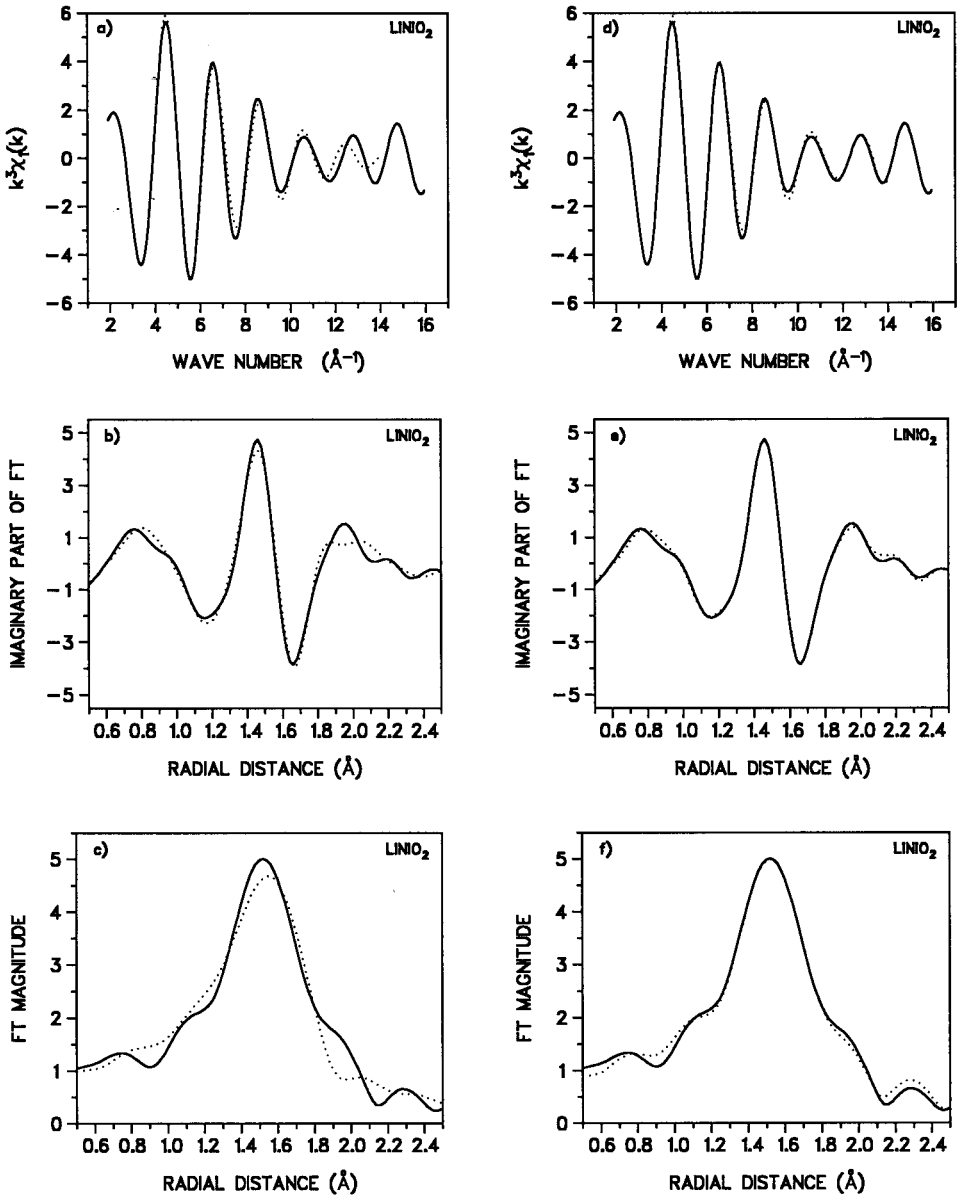


**Figure 7.** Experimental filtered data (solid curve) and calculated fit data (dotted curve) for $LiNiO_2$: a−c correspond to $k^3\chi_1$, imaginary part of FT, and magnitude of FT, respectively, using a single-shell fit employing Ni−O theoretical standards; d−f correspond to $k^3\chi_1$, imaginary part of FT, and magnitude of FT, respectively, using a two-shell fit employing Ni−O theoretical standards with $N_1 = 4$ and $N_2 = 2$.

the nickel backscatterers was set to be equal to 6, as determined from the X-ray diffraction data. Results for *k*-weightings of 1, 2, and 3 show that the fits converged for $N_1$ values around 4 and $N_2$ values around 2 with distances similar to those obtained from the two-shell fit to the filtered $\chi_1(k)$ data. Next, to examine the validity of the assumption that all oxygen atoms have the same disorder, we set $N_1$ and $N_2$ to be equal to 4 and 2, respectively, and assumed that each subshell of oxygen atoms has a different disorder. It can be seen from estimates of the sum of the square of residuals that the quality of this fit is similar to the one in which the disorder for all oxygen atoms was assumed to be the same; the results of both fits look acceptable. Results of this latter fit show that disorders for the two subshells of oxygen atoms are roughly the same and are comparable to those of the former fit especially for *k*-weighting exponents of 2 and 3.

The local structure of the first shell of Ni in $LiNiO_2$ consists of four oxygen atoms at 1.91 Å and two oxygen atoms at 2.06 Å, which is contrary to XRD results (Table 1). The second coordination sphere consists of six nickel atoms at distance of 2.87 Å. Our EXAFS results are consistent with the results of a recent EXAFS study by Rougier, Delmas, and Chadwick[61] which gives four and two oxygen atoms at 1.91 and 2.09 Å, respectively, and six nickel atoms at 2.87 Å, as deduced from EXCURV92 analysis procedure. In this study, the distorted octahedral coordination was interpreted in terms of a Jahn−Teller effect of trivalent nickel in the low spin state. Later in the text, we provide an alternative mechanism for the local distortion based on oxygen holes. The average Ni−O bond length of 1.96 Å (from our EXAFS results) is consistent with the average Ni−O bond length extrapolated for $x = 0.5$ based on results of a neutron diffraction study of $Li_xNi_{(1-x)}O$ for $x$ values in the range 0.15−0.4 by Pickering et al.[62] On the basis of the ionic radii of $Ni^{2+}$, low-spin $Ni^{3+}$, and $Li^+$ and the neutron diffraction results, Pickering et al. concluded that Ni in $Li_xNi_{(1-x)}O$ is present as $Ni^{2+}$ and $Ni^{3+}$ in proportions varying with $x$. More recently, two Ni−O bond lengths (1.91 and 2.06 Å) which are independent of composition were observed in an EXAFS study of $Li_xNi_{(1-x)}O$ for $x$ values in the range 0.15−0.4 by Pickering et al.[62] In this study, the data were interpreted

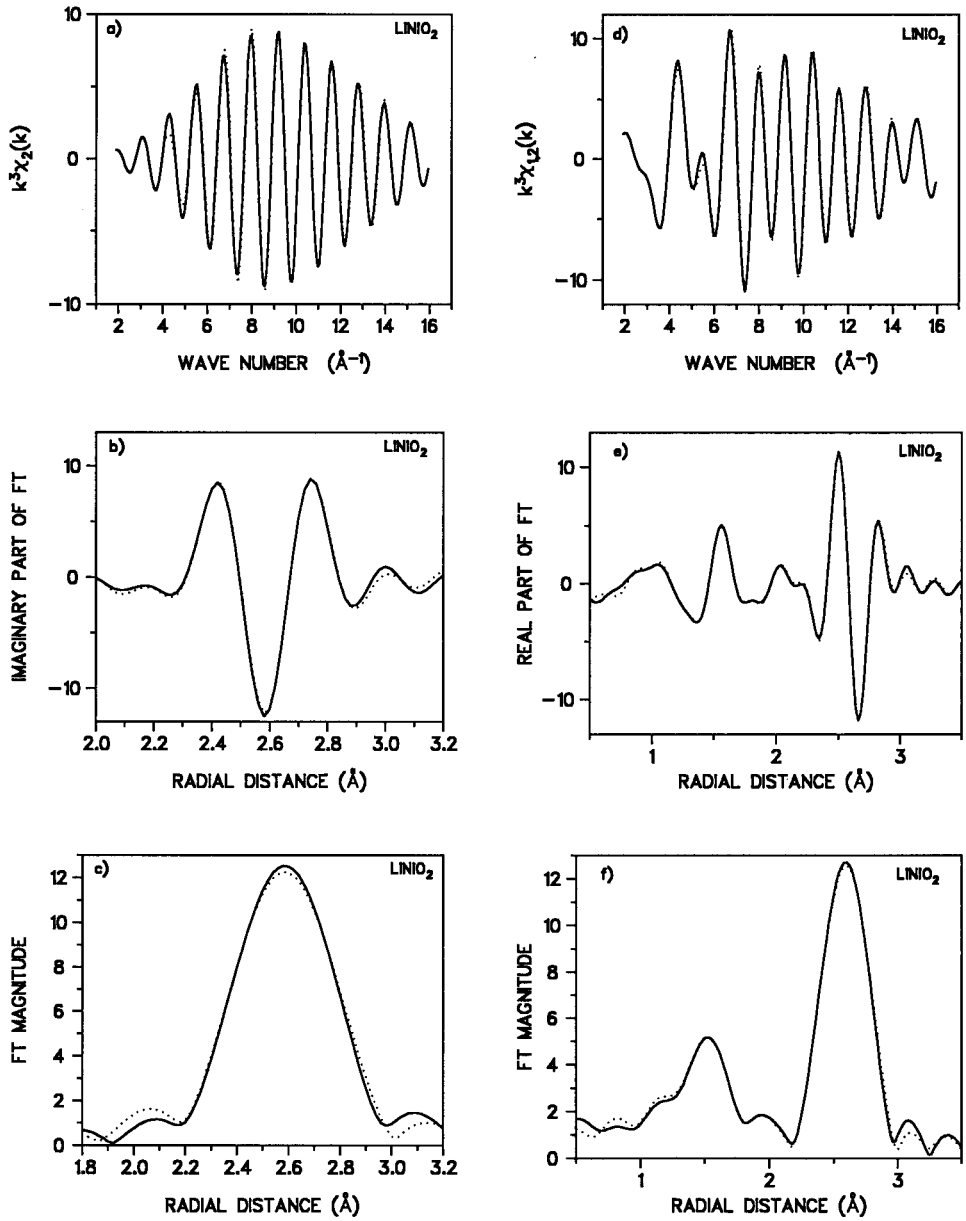


**Figure 8.** Experimental filtered data (solid curve) and calculated fit data (dotted curve) for $LiNiO_2$: a−c correspond to $k^3\chi_2$, imaginary part of FT, and magnitude of FT, respectively, using single-shell employing Ni−Ni theoretical standards; d−f correspond to $k^3\chi_{1,2}$, imaginary part of FT, and magnitude of FT, respectively, using three-shell, two-shell (for the first FT peak) with Ni−O theoretical standards, and one shell (for the second FT peak) with Ni−Ni theoretical standards.

in terms of two different models. Model 1 assumed that the holes reside on the Ni atoms, and hence, $Ni^{3+}-O^{2-}$ (short distance) and $Ni^{2+}-O^{2-}$ (long distance) bonds with proportions varying with $x$ should be present. Model 2 assumed that the holes reside on the oxygen atoms, and hence, $Ni^{2+}-O^{-}$ (short distance) and $Ni^{2+}-O^{2-}$ (long distance) bonds with proportions changing with $x$ should be present. In this study, model 1 was marginally favored. According to model 1, for $x = 0.5$ (i.e., $LiNiO_2$), only $Ni^{3+}-O^{2-}$ bonds should be present, and hence, only the short Ni−O distance should be observed. Based on model 2, for $x = 0.5$ one should observe three $Ni^{2+}-O^{-}$ (short distance) and three $Ni^{2+}-O^{2-}$ (long distance) bonds. Assuming that the density of holes on oxygen is 0.7, as pointed out by Kuiper et al.,[42] model 2 predicts that the number of $Ni^{2+}-O^{-}$ bonds is 2.1 and the number of $Ni^{2+}-O^{2-}$ bonds should also be 2.1. Since, the remainder of the holes must reside on the nickel atoms, model 1 predicts that the number of $Ni^{3+}-O^{2-}$ bonds is 1.8. Accordingly, the total number of short bonds is 3.9 and the number of long bonds is 2.1; these are in excellent agreement with our EXAFS results. Our results are thus consistent with the fact that the charge-compensating mechanism largely is due to holes residing on the oxygen atoms rather than the nickel atoms, in agreement with results based on the O K-edge spectra. An estimate for the average nickel valency can be determined from the number of $Ni^{3+}-O^{2-}$ bonds, which gives 2.3. This average valency is less than that estimated on the basis of edge energies, which is in the range 2.58−2.99. Thus, our XANES data (Figure 2) suggest that the edge energy is sensitive to changes in the electronic structure regardless of whether the holes reside on the nickel or the oxygen atoms since the $Ni^{2+}-O^{-}$ bond length is the same as the $Ni^{3+}-O^{2-}$ bond length. Taking into account the number of both the $Ni^{3+}-O^{2-}$ and $Ni^{2+}-O^{-}$ gives an effective valency for nickel of 2.7, which is in excellent agreement with estimates based on the edge energies. It is the distance of the Ni−O bond that alters the

**TABLE 8: Local Structure Parameters for $KNiIO_6$**

| filtered data | $W$ | X-Y pair | $S_0^2$ | $N$ | $R$ (Å) | $\delta R$ (Å) | $\Delta\sigma^2$ ($10^{-3}$ Å$^2$) | $\Delta E_0$ (eV) | SSR |
|---|---|---|---|---|---|---|---|---|---|
| $\chi_1$, M1 | 3 | Ni−O | 0.74 | 6 | 1.879 | | 3.4 | −9.8 | 37.5 |
| $\chi_1$, M2 | 3 | Ni−O | 0.73 | 6 | 1.878 | | 3.3 | −9.8 | 39.1 |
| $\chi_1$, M4 | 3 | Ni−O | 0.72 | 6 | 1.878 | | 3.2 | −8.9 | 36.4 |
| $\chi_1$, M5 | 3 | Ni−O | 0.86 | 6 | 1.877 | | 3.8 | −9.5 | 29.5 |
| | 2 | Ni−O | 0.83 | 6 | 1.878 | | 3.5 | −9.7 | 0.61 |
| | 1 | Ni−O | 0.81 | 6 | 1.875 | | 3.3 | −9.4 | 0.018 |
| $\chi_2$, M5 | 3 | Ni−I | 0.73 | 3 | 2.869 | 0.000 | 1.8 | −6.9 | 71.4 |
| $\chi_2$, M5 | 3 | Ni−I | 0.71 | 3 | 2.864 | −0.005 | 1.7 | −5.4 | 6.9 |
| | | Ni−O | | 6 | 3.586 | | 4.1 | −13.0 | |
| | 2 | Ni−I | 0.71 | 3 | 2.864 | −0.005 | 1.7 | −5.3 | 0.12 |
| | | Ni−O | | 6 | 3.597 | | 3.8 | −14.0 | |
| | 1 | Ni−I | 0.68 | 3 | 2.865 | −0.004 | 1.5 | −5.6 | 0.004 |
| | | Ni−O | | 6 | 3.604 | | 2.8 | −14.2 | |
| $\chi_{1,2}$, M5 | 3 | Ni−O | 0.78 | 6 | 1.876 | | 3.3 | −9.0 | 46.4 |
| | | Ni−I | | 3 | 2.866 | −0.003 | 2.1 | −6.0 | |
| | | Ni−O | | 6 | 3.556 | | 4.6 | −9.0 | |
| | 2 | Ni−O | 0.78 | 6 | 1.876 | | 3.1 | −8.8 | 1.01 |
| | | Ni−I | | 3 | 2.866 | −0.003 | 2.1 | −6.1 | |
| | | Ni−O | | 6 | 3.538 | | 5.3 | −8.8 | |
| | 1 | Ni−O | 0.81 | 6 | 1.872 | | 3.2 | −8.2 | 0.026 |
| | | Ni−I | | 3 | 2.870 | +0.001 | 2.4 | −6.7 | |
| | | Ni−O | | 6 | 3.504 | | 8.0 | −8.2 | |

[a] $N$: coordination number. $R$: coordination distance. $\sigma^2$: mean square relative displacement, $\Delta E_0$: inner potential correction. $W$: $k$-weighting exponent. SSR: sum of the square of residuals between experimental and calculated spectra. Fits were performed using theoretical standards generated from structure data for NiO (model M1), $\beta$-$Ni(OH)_2$ (model M2), and $KNiIO_6$ with structure data from ref 29 (model M4) or refs 27 and 28 (model M5). All fits were refined over the $k$-range 4−14 Å$^{-1}$.

edge energy regardless of whether the change in distance is due to holes on the nickel or the oxygen atoms.

**$KNiIO_6$.** Analysis was made using theoretical standards generated from structure data for NiO, $\beta$-$Ni(OH)_2$, and $KNiIO_6$. A summary of the results is listed in Table 8. Comparisons of calculated and experimental spectra are shown in Figure 9. A single-shell fit to the filtered $\chi_1(k)$ data using theoretical standards generated from structure data for NiO, $\beta$-$Ni(OH)_2$, and $KNiIO_6$ (ref 29 for $KNiIO_6$) yielded essentially the same results and the same quality of fits with roughly the same value for the sum of the square of residuals. An $S_0^2$ value of roughly 0.73, with only a weak dependence on the $k$-weighting exponent, was obtained. The quality of the single-shell fit was improved when a theoretical standard generated using more recent structure data for $KNiIO_6$ (refs 27 and 28) was used. The more recent X-ray diffraction structure data give a Ni−O distance of 1.80 Å, which is closer to the true distance than the 2.18 Å distance obtained from earlier results (Table 1). Therefore, we have adapted the theoretical standards generated using the most recent structure data for the analysis of the first, second, and third coordination spheres. A single-shell fit (Figure 9a,b,c) yielded an $S_0^2$ value of 0.86 compared to 0.74 for the other models. Note that the distance remained the same regardless of whether theoretical standards generated from structure data for NiO, $\beta$-$Ni(OH)_2$, or $KNiIO_6$ were used. A single-shell fit to the filtered $\chi_2(k)$ data using Ni−I theoretical standards yielded a very poor fit. The quality of the fit was improved significantly when the contribution of the third coordination sphere of oxygen atoms was included. A reduction in the sum of the square of residuals by a factor of 10 was obtained. Comparisons of calculated and experimental spectra are shown in Figure 9 (d, e, and f). An $S_0^2$ value of 0.71 was obtained, compared to the value of 0.86 obtained from the fit to the $\chi_1(k)$ data. The Ni−I second-shell distance of 2.864 Å is consistent with the distance determined from X-ray diffraction. The Ni−O distance for the third shell of oxygen atoms of 3.60 Å is, however, significantly larger than that based on the X-ray diffraction data. Note that the inner potential for the third shell of oxygen atoms differs significantly from that for the first shell of oxygen atoms, which should not be the case. Therefore, a fit to the $\chi_{1,2}(k)$ data, in which the inner potential for the third shell of oxygen atoms was constrained to that for the first shell of oxygen atoms, was made. This fit gives a many-body amplitude reduction factor, $S_0^2$, of 0.78, which is similar to that obtained for metallic nickel and nearly is independent of the $k$-weighting exponent. The Ni−O first-shell distance was the same as that obtained from the single-shell fit to the filtered $\chi_1(k)$ data, and the Ni−I second-shell distance was the same as that obtained from the two-shell fit to the filtered $\chi_2(k)$ data. The Ni−O third-shell distance was, however, smaller than that obtained from the two-shell fit to the filtered $\chi_2(k)$ data and is now closer to that based on the X-ray diffraction data.

A summary of local structure parameters obtained from averaging the most reliable results listed in Tables 3−8 is shown in Table 9. In Figure 10, we show the dependence of the first-shell Ni−O bond length on nickel valency. The solid curve is a quadratic polynomial fit (used here to guide the eye). Clearly, the Ni−O bond length decreases with increase in nickel valency in a nonlinear manner. We would like to point out that if one assumes that all of Ni in $LiNiO_2$ is present as $Ni^{3+}$ with a distorted octahedral coordination as proposed by Rougier, Delmas, and Chadwick[61] and the average of the short and long distances is taken to be characteristic of $Ni^{3+}$, then the Ni−O bond length decreases linearly with increase in Ni valency, as we have shown in an earlier publication.[63]

## Conclusions

In general, we can make the following remarks. Local structure analysis should always be made at least at $k$- and $k^3$-weighting. Large variations in local structure parameters (such as $S_0^2$, $N$, $R$, $\sigma^2$) as a function of the $k$-weighting exponent can point out important structural information. We present here two examples: first, the need for an asymmetric distribution function instead of a Gaussian distribution function to model disorder as is the case for the Ni−Ni contribution in α-$Ni(OH)_2$; second, the need to include the contribution of the third shell of oxygen atoms in addition to the Ni−Ni and Ni−I when analyzing the

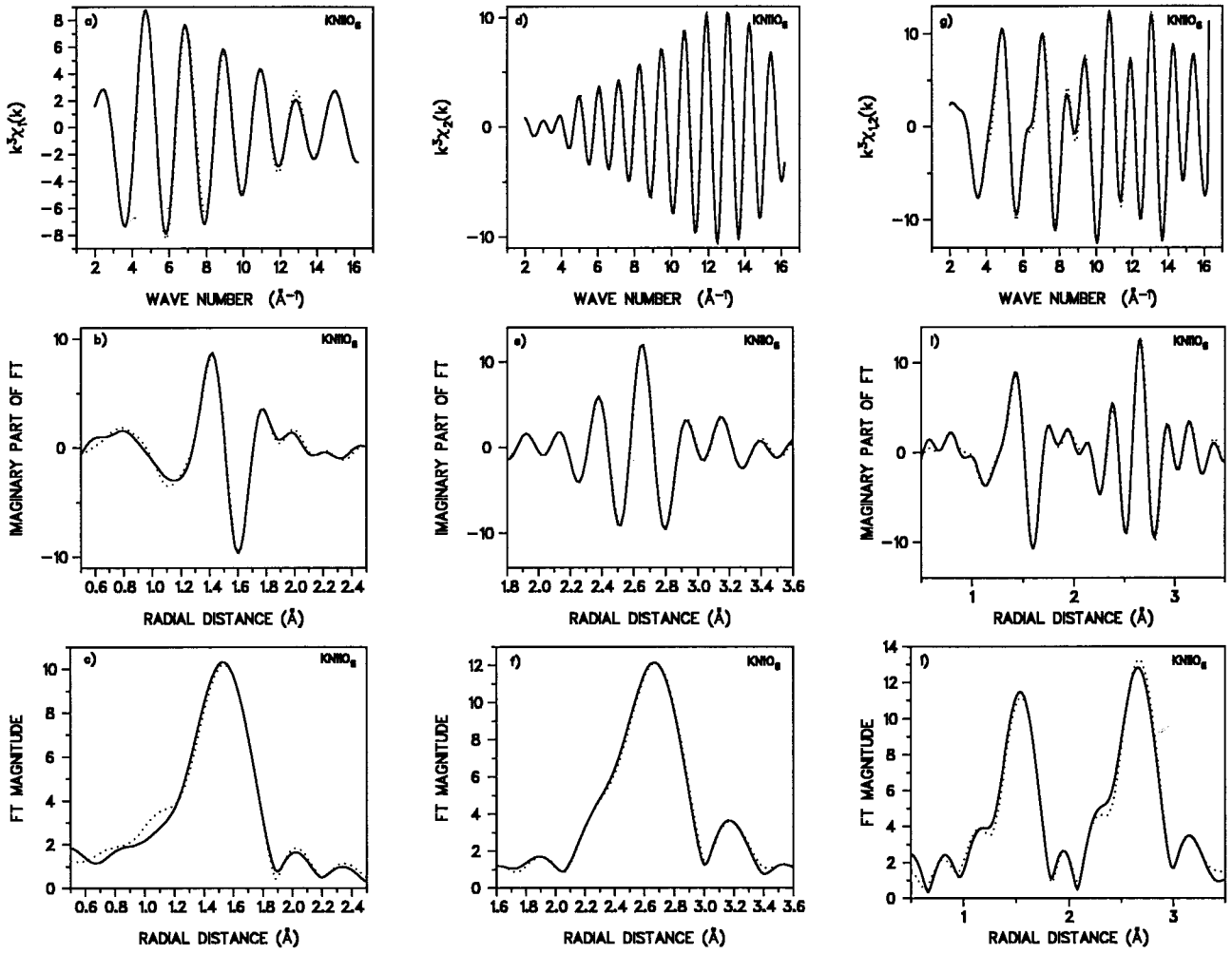


**Figure 9.** Experimental filtered data (solid curve) and calculated fit data (dotted curve) for $KNiIO_6$: a−c correspond to $k^3\chi_1(k)$, imaginary part of FT, and magnitude of FT, respectively, using one shell of Ni−O; d−f correspond to $k^3\chi_2$, imaginary part of FT, and magnitude of FT, respectively, using one shell of Ni−I and one shell of Ni−O; g, h, and f correspond to $k^3\chi_{1,2}$, imaginary part of FT, and magnitude of FT, respectively, using two shells of Ni−O and one shell of Ni−I.

**TABLE 9: Summary of Local Structure Data for Various Nickel Compounds Obtained by Averaging Most Reliable Results Listed in Tables 3−8. The Errors Quoted Are the "*n*−1" Standard DeviationCompound**

| compound | X-Y pair | $S_0^2$ | N | $R$, Å | $\delta R$, Å | $\sigma^2$, $10^{-3}$ Å$^2$ | $C_3$, $10^{-4}$ Å$^3$ | $C_4$, $10^{-5}$ Å$^4$ |
|---|---|---|---|---|---|---|---|---|
| Ni | Ni−Ni | $0.77 \pm 0.02$ | 12 | $2.479 \pm 0.001$ | −0.013 | $5.4 \pm 0.2$ | | |
| NiO | Ni−O | $0.78 \pm 0.14$ | 6 | $2.074 \pm 0.003$ | −0.015 | $3.5 \pm 1.1$ | | |
| | Ni−Ni | | 12 | $2.949 \pm 0.005$ | −0.005 | $5.6 \pm 0.8$ | | |
| | Ni−O | | 8 | $3.609 \pm 0.008$ | −0.008 | $9.7 \pm 4.4$ | $24.1 \pm 10.3$ | $11.5 \pm 9.1$ |
| $\beta$-$Ni(OH)_2$ | Ni−O | $0.76 \pm 0.07$ | 6 | $2.063 \pm 0.005$ | −0.010 | $4.9 \pm 0.5$ | | |
| | Ni−Ni | | 6 | $3.128 \pm 0.002$ | +0.002 | $6.2 \pm 0.5$ | | |
| $\alpha$-$Ni(OH)_2$ | Ni−O | $0.80 \pm 0.14$ | 6 | $2.037 \pm 0.004$ | | $6.5 \pm 0.3$ | | |
| | Ni−Ni | | 6 | $3.133 \pm 0.000$ | | $13.3 \pm 2.6$ | $4.5 \pm 0.1$ | $9.8 \pm 3.9$ |
| $LiNiO_2$ | Ni−O | $0.71 \pm 0.07$ | 4 | $1.914 \pm 0.010$ | | $4.5 \pm 0.8$ | | |
| | Ni−O | | 2 | $2.061 \pm 0.021$ | | $4.8 \pm 1.7$ | | |
| | Ni−Ni | | 6 | $2.873 \pm 0.004$ | −0.005 | $4.2 \pm 0.6$ | | |
| $KNiIO_6$ | Ni−O | $0.77 \pm 0.06$ | 6 | $1.876 \pm 0.002$ | | $3.4 \pm 0.3$ | | |
| | Ni−I | | 3 | $2.866 \pm 0.002$ | −0.003 | $1.9 \pm 0.4$ | | |
| | Ni−O | | 6 | $3.564 \pm 0.039$ | | $4.8 \pm 1.8$ | | |

second peak in the Fourier transforms of NiO and $KNiIO_6$, respectively. This is an important result that shows that the second peak in the Fourier transforms of NiO and $KNiIO_6$ does not represent a single-shell contribution and, hence, should not be used to extract empirical standards for Ni−Ni and Ni−I atom pairs. The effect of theoretical standards generated using different structure models (such as NiO vs $\beta$-$Ni(OH)_2$) on local structure parameters is very weak. The Ni−O and Ni−Ni bond lengths are almost invariant when different structure models are used. The greatest variations were observed in the values of $S_0^2$ and $\sigma^2$. Most reliable results were obtained when analysis was made on combined contributions of two or three shells rather than a single-shell contribution. Our results indicate that the inner potential parameter depends very weakly on the type of backscattering atoms (such as oxygen vs nickel). In most cases, at least for nickel oxides, one inner potential parameter is sufficient for analyzing all shells. It is also reasonable to assume that the many-body amplitude reduction factor is shell independent. An $S_0^2$ of $0.77 \pm 0.03$ for Ni K-edge absorption

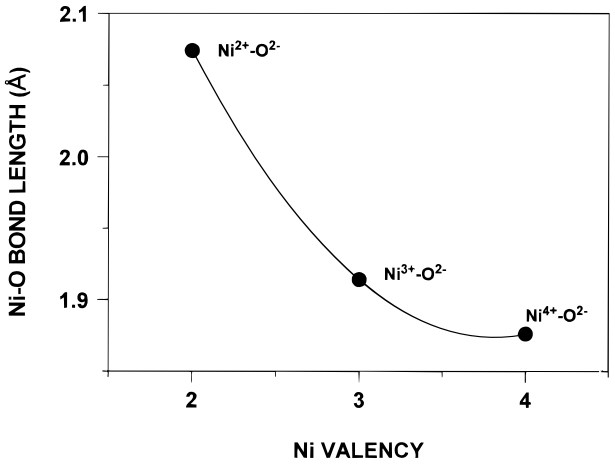


**Figure 10.** Ni−O bond length as a function of nickel valency. The solid curve is a quadratic polynomial fit to the data used to guide the eye.

can be used to scale theoretical spectra to fit the experimental ones in order to accurately determine the coordination numbers for compounds with complex structures. Our results show that chemical effects are very small and can be ignored for reliable structural analysis. The Ni−O bond lengths of the first coordination sphere obtained using theoretical standards are usually slightly shorter (≈0.015 Å) than those obtained from well-established X-ray or neutron diffraction data. This is also true for the Ni−Ni first-shell distance of metallic nickel. The Ni−Ni and Ni−I bond lengths are in agreement with bond lengths determined from X-ray or neutron diffraction data. The local structure, within the hexagonal planes, for α-$Ni(OH)_2$ is similar to that for $\beta$-$Ni(OH)_2$. The apparent contraction in the Ni−Ni distance for α-$Ni(OH)_2$ compared to that for $\beta$-$Ni(OH)_2$ is not real but is due to structural disorder. The first coordination sphere of $LiNiO_2$ consists of four oxygens at 1.91 and two oxygens at 2.06 Å. The short distance is due to the presence of $Ni^{3+}-O^{2-}$ and $Ni^{2+}-O^{-}$ bonds, while the long distance is due to the presence of $Ni^{2+}-O^{2-}$ bonds. This model is preferred over that proposed by Rougier, Delmas, and Chadwick[61] (which assumes the distortion is due to a Jahn−Teller effect), because it is also consistent with oxygen K-edge data which show that the charge-compensating mechanism for $LiNiO_2$ mainly is due to holes residing on the oxygen atoms. Quadrivalent Ni has a characteristic Ni−O bond length of 1.88 Å, which is significantly shorter than that for divalent and trivalent nickel. We have derived three calibration curves based on the Ni−O bond length, the X-ray edge energy and the preedge peak energy to aid in the determination of nickel valency in materials with complex structures such as the charged and discharged products of the nickel oxide electrode. The Ni−O bond length decreased with increase in nickel valency in a nonlinear manner. Both the Ni K-edge energy and the preedge peak energy increased with increase in nickel valency.

In summary, we have measured the room-temperature X-ray absorption spectra of Ni, NiO, α- and $\beta$-$Ni(OH)_2$, $LiNiO_2$, and $KNiIO_6$. The local structure of nickel up to the third coordination sphere was successfully analyzed using theoretical standards generated with FEFF code (version 5.0). Within the analyzed region, only SS contributions were essential for reliable structural analysis. Variations in the X-ray edge energies, preedge peak energies, and the Ni−O bond length as a function of nickel valency were established.

**Acknowledgment.** The authors acknowledge financial support by the Office of Naval Research, Chemistry Division, under Contract No. N0001496WX20162, and the NSWCCD ILIR Program (ANM) and the U.S. Department of Energy, Materials Science Division (CAM). The support of the U.S. Department of Energy, Division of Materials Sciences, under Contract No. DE-AS05-80-ER-10742 for its role in the development and operation of beamline X-11A at the National Synchrotron Light Source (NSLS) is also acknowledged. The NSLS is supported by the Department of Energy, Division of Materials Sciences and Division of Chemical Sciences, under Contract No. DE-AC02-76CH00016. We are thankful to Drs. L. Xie of Rayovac Corp. for providing the $LiNiO_2$ sample and S. Dallek of NSWCCD for performing thermogravimetric analysis on our α-$Ni(OH)_2$ sample.

## References and Notes

(1) Oliva, P.; Leonardi, J.; Laurent, J. F.; Delmas, C.; Braconier, J. J.; Figlarz, M.; Fievet, M.; de Guibert, A. *J. Power Sources* **1982**, *8*, 229.
(2) McBreen, J. M.; O'Grady, W. E.; Pandya, K. I. *J. Power Sources* **1988**, *22*, 323.
(3) Crespin, M.; Levitz, P.; Gatineau, L. *J. Chem. Soc., Faraday Trans. 2* **1983**, *79*, 1181.
(4) Crespin, M.; Levitz, P.; Gatineau, L. *J. Chem. Soc., Faraday Trans. 2* **1983**, *79*, 1195.
(5) McBreen, J.; O'Grady, W. E.; Pandya, K. I.; Hoffman, R. W.; Sayers, D. E. *Langmuir* **1987**, *3*, 931.
(6) Pandya, K. I.; Hoffman, R. W.; McBreen, J.; O'Grady, W. E. *J. Electrochem. Soc.* **1990**, *137*, 383.
(7) McBreen, J.; O'Grady, W. E.; Tourillon, G.; Dartyge, E.; Fontaine, A.; Pandya, K. I. *J. Phys. Chem.* **1989**, *93*, 6308.
(8) Pandya, K. I.; O'Grady, W. E.; Corrigan, D. A.; McBreen, J.; Hoffman, R. W. *J. Phys. Chem.* **1990**, *94*, 21.
(9) Capehart, T. W.; Corrigan, D. A.; Conell, R. S.; Pandya K. I.; Hoffman, R. W. *Appl. Phys. Lett.* **1991**, *58*, 865.
(10) Mansour, A. N.; Melendres, C. A.; Pankuch, M.; Brizzolara, R. A. *J. Electrochem. Soc.* **1994**, *141*, L69.
(11) Mansour, A. N.; Melendres, C. A.; Pankuch, M.; Brizzolara, R. *The Electrochem. Soc. Extended Abstr.* **1994**, *94−1*, 60.
(12) Mansour, A. N.; Melendres, C. A. *Electrochem. Soc. Extended Abstr.* **1994**, *94−2*, 229.
(13) Mansour, A. N.; Melendres, C. A. *Physica B* 1995, *208&209*, 583.
(14) Curie, D. B.; Levason, W.; Oldroyd, R. D.; Weller, M. T. *J. Chem. Soc., Dalton Trans.* **1994**, 1483.
(15) O'Grady, W. E.; Pandya, K. I.; Swider, K. E.; Corrigan, D. A. *J. Electrochem. Soc.* **1996**, *143*, 1613.
(16) Glemser, D. *Handbook of Preparative Inorganic Chemistry*; Academic Press: London, 1965; Vol. 2, p 1549.
(17) Xie, L.; Eboner, W.; Foucchard, D.; Megahead, S. *Electrochem. Soc. Extended Abstr.* **1994**, *94−2*, 162.
(18) Murthy, C. P.; Sethuram B.; Rao, T. N. *Z. Phys. Chem. (Leipzig)* **1986**, *267*, 1212.
(19) Ohzuku T.; Ueda A.; Nagayama M. *J. Electrochem. Soc.* **1993**, *140*, 1862.
(20) Wyckoff, R. W. G. *Crystal Structures*, 2nd ed.; Interscience: New York, 1963; Vol. 1, p 10.
(21) Villars, P.; Calver, L. D. *Persons Handbook of Crystallographic Data for Intermetallic Phases*, American Society for Metals, Metals Park, OH, 1985; Vol. 3, p 2864.
(22) Greaves, C.; Thomas, M. A. *Acta Crystallogr.* **1986**, *B52*, 51.
(23) McEwen, R. S. *J. Phys. Chem.* **1971**, *75*, 1782.
(24) Bode, H.; Dehmelt K.; Witte, J. *Electrochim. Acta* **1966**, *11*, 1079.
(25) Wyckoff, R. W. G. *Crystal Structures*, 2nd ed.; Interscience: New York, **1964**, Vol. 2, p 292.
(26) Dyer, L. D.; Borie, B. S., Jr.; Smith, G. P. *J. Am. Chem. Soc.* **1954**, *76*, 1499.
(27) Vannerberg, N. G.; Blockhammar, I. *Acta Chem. Scand.* **1965**, *19*, 875.
(28) Eddy L. P.; Vannerberg, N.-G. *Acta Chem. Scand.* **1966**, *20*, 2886.
(29) Currie, D. B.; Levason, W.; Oldroyd, R. D.; Teller, M. T. *J. Mater. Chem.* **1993**, *3*, 44.
(30) Pickering, I. J.; Lewandowski, J. T.; Jacobson, A. J.; Goldstone, J. A. *Solid State Ionics* **1992**, *53−56*, 405.
(31) Sayers, D. E.; Heald, S. M.; Pick, M. A.; Budnick, J. I.; Stern, E. A.; Wong, J. *Nucl. Instrum. Methods Phys. Res.* **1983**, *208*, 631.
(32) Lu K.-Q.; Stern, E. A. *Nucl. Instrum. Methods* **1983**, *212*, 475.
(33) Stern, E. A.; Kim, K. *Phys. Rev. B* **1981**, *23*, 3781.
(34) Sayers, D. E.; Bunker, B. A. *X-ray Absorption: Principles, Applications, Techniques of EXAFS, SEXAFS and XANES*; Koningsberger, D. C., Prins, R., Eds.; Wiley: New York, 1988; Chapter 6.

(35) Cook, Jr., J. W.; Sayers, D. E. *J. Appl. Phys.* **1981**, *52*, 5024.
(36) The bulk of the analysis was made using the XAFS data analysis package of the Eindhoven University of Technology (developed by Diek Koningsberger and co-workers).
(37) McMaster, W. H.; Kerr Del Grande, N.; Mallet, J. H.; Hubbell, J. H. *Compilation of X-ray Cross Sections*; National Technical Information Services: Springfield, VA, 1969.
(38) Cotton, F. A.; Wilkinson, G. *Advanced Inorganic Chemistry*; Interscience: New York, 1966; p 891.
(39) Hewston, T. A.; Chamberland, B. L. *J. Phys. Chem. Solids* **1987**, *48*, 97.
(40) Li, W.; Reimers, J. N.; Dahn, J. R. *Phys. Rev. B* **1992**, *46*, 3236.
(41) Reimers, J. N.; Li, W.; Dahn, J. R. *Phys. Rev. B* **1993**, *47*, 8486.
(42) Kuiper, P.; Kruizinga, G.; Ghijsen, J.; Sawatzky, G. A. *Phys. Rev. Lett.* **1989**, *62*, 221.
(43) van Elp, J.; Eskes, H.; Kuiper, P.; Sawatzky, G. A. *Phys. Rev. B* **1992**, *45*, 1612.
(44) Oku, M.; Tokuda, H.; Hirokawa, K. *J. Electron Spectrosc. Relat. Phenom.* **1991**, *53*, 201.
(45) Abbate, M.; de Groot, F. M. F.; Fuggle, J. C.; Fujimori, A.; Tokura, Y.; Fujishima, Y.; Strebel, O.; Domke, M.; Kaindl, G.; van Elp, J.; Thole, B. T.; Sawatzky, G. A.; Sacchi, M.; Tsuda, N. *Phys. Rev. B* **1991**, *44*, 5419.
(46) van Elp, J.; Searle, B. G.; Sawatzky, G. A. *Solid State Commun.* **1991**, *80*, 67.
(47) van Veenendaal, M. A.; Sawatzky, G. A. *Phys. Rev. B* **1994**, *50*, 11326.
(48) Boyce, J. B.; Bridges, F.; Claeson, T.; Howland, R. S.; Geballe, T. H. *Phys. Rev. B* **1987**, *36*, 5251.
(49) Yarmoff, J. A.; Clarke, D. R.; Drube, W.; Karlsson, U. O.; Taleb-Ibrahimi, A.; Himpsel, F. J. *Phys. Rev. B* **1987**, *36*, 3967.
(50) Bunker, G. *Nucl. Instrum. Methods Phys. Res.* **1983**, *207*, 437.
(51) Zabinsky, S. I.; Rehr, J. J.; Ankudinov, A.; Albers, R. C.; Eller, M. J. *Phys. Rev. B* **1995**, *52*, 2995.
(52) Zabinsky, S. I.; Rehr, J. J.; Ankudinov, A.; Albers, R. C.; Eller, M. J. *Phys. Rev. B* **1995**, *52*, 2995.
(53) Stern, E. A. *Phys. Rev. B* **1993**, *48*, 9825.
(54) Lytle, F. W.; Sayers, D. E.; Stern, E. A. *Physica B* **1989**, *158*, 701.
(55) *(55) X-ray Absorption Fine Structure*; Hasnain, S. S., Ed.; Ellis Horwood: Chichester, UK, 1991; Chapter 195.
(56) Li, G. G.; Bridges, F.; Booth, C. H. *Phys. Rev. B* **1995**, *52*, 6332.
(57) Touloukian, Y. S.; Kirby, R. K.; Taylor, R. E.; Lee, T. Y. R.; *Thermophysical Properties of Matter*, *The TPRC Data Series*; Plenum Publishing Co.: New York, 1997; Vol. 13, p 42a.
(58) Mansour, A. N. Unpublished results.
(59) Haskel, D.; Ravel, B.; Newville, M.; Stern, E. A. *Physica B* **1995**, *208 & 209*, 151.
(60) Kuzmin, K.; Mironova, N.; Purans, J.; Rodionov, A. *J. Phys.: Condens. Matter* **1995**, *7*, 9357.
(61) Rougier, A.; Delmas, C.; Chadwick, A. V. *Solid State Commun.* **1995**, *94*, 123.
(62) Pickering, I. J.; George, G. N.; Lewandowski, J. T.; Jacobson, A. J. *J. Am. Chem. Soc.* **1993**, *115*, 4137.
(63) Mansour, A. N.; Melendres, C. A. *J. Phys. IV* **1997**, *7*, C2−1171.